DESIGN OF SMART ANTENNA ARRAY FOR INTERFERENCE SUPPRESSION IN GPS

A THESIS SUBMITTED TO
THE GRADUATE SCHOOL OF NATURAL AND APPLIED SCIENCES
OF
MIDDLE EAST TECHNICAL UNIVERSITY

BY

ÖMER CAN DABAK

IN PARTIAL FULFILLMENT OF THE REQUIREMENTS
FOR
THE DEGREE OF MASTER OF SCIENCE
IN
ELECTRICAL AND ELECTRONICS ENGINEERING

JUNE 2016

Approval of the thesis:

DESIGN OF SMART ANTENNA ARRAY FOR INTERFERENCE SUPPRESSION IN GPS

submitted by **ÖMER CAN DABAK** in partial fulfillment of the requirements for the degree of **Master of Science in Electrical and Electronics Engineering Department, Middle East Technical University** by,

Prof. Dr. Gülbin Dural Ünver
Dean, Graduate School of **Natural and Applied Sciences** _____

Prof. Dr. Gönül Turhan Sayan
Head of Department, **Electrical and Electronics Eng.** _____

Assoc. Prof. Dr. Lale Alatan
Supervisor, **Electrical and Electronics Eng. Dept.,METU** _____

Prof. Dr. S.Sencer Koç
Co-Supervisor,**Electrical and Electronics Eng. Dept.,METU** _____

Examining Committee Members:

Prof. Dr. Özlem Aydın Çivi
Electrical and Electronics Eng. Dept.,METU _____

Assoc. Prof. Dr. Lale Alatan
Electrical and Electronics Eng. Dept.,METU _____

Prof. Dr. S. Sencer Koç
Electrical and Electronics Eng. Dept.,METU _____

Prof. Dr. Çağatay Candan
Electrical and Electronics Eng. Dept.,METU _____

Assoc. Prof. Dr. Vakur B. Ertürk
Electrical and Electronics Eng. Dept.,Bilkent University _____

Date: 30.06.2016

I hereby declare that all information in this document has been obtained and presented in accordance with academic rules and ethical conduct. I also declare that, as required by these rules and conduct, I have fully cited and referenced all material and results that are not original to this work.

Name, Last name: Ömer Can DABAK

Signature:

ABSTRACT

DESIGN OF SMART ANTENNA ARRAY FOR INTERFERENCE SUPPRESSION IN GPS

Dabak, Ömer Can

M.S.,Department of Electrical and Electronics Engineering

Supervisor: Assoc. Prof. Dr. Lale Alatan

Co-Supervisor: Prof. Dr. S.Sencer Koç

June 2016, 79 pages

GPS jammers add excessive noise to received low power GPS signals and have capability to weaken or completely destroy the positioning performance of GPS receivers. The most popular technique to overcome GPS jamming problem is suppression of jammers by using array signal processing techniques. In this thesis, a GPS anti-jamming system is constructed by designing an active antenna array and implementing adaptive beamforming techniques. This thesis mainly include the design of four element active circularly polarized microstrip antenna array, implementation of beamforming techniques and presentation of experimental results obtained from the constructed GPS anti-jamming system. In active antenna array design, circularly polarized operation of the array element is achieved through nearly square microstrip patch antenna structure. After verification of the design by comparing simulation and measurement results, four element planar array is designed and manufactured. Then, four channel LNA card design and production is performed in order to obtain a compact active antenna array. All electromagnetic simulation and parametric analysis of the antennas are performed in electromagnetic simulation tool CST Microwave Studio. In beamforming section, two main beamforming methods that are Capon beamforming and null steering are studied with theory and simulation results obtained from the code developed in MATLAB environment. The jammer suppression success of the constructed system is demonstrated by scenarios that include real satellites and a continuous wave jammer source.

KEYWORDS: Nearly Square Microstrip Antenna, Circular Polarization, Antenna Array, Beamforming, GPS antijamming

ÖZ

GPS SİSTEMLERİNDE GİRİŞİM BASKILAMAK İÇİN AKILLI ANTEN TASARIMI

Dabak, Ömer Can

Yüksek Lisans, Elektrik ve Elektronik Mühendisliği Bölümü

Tez Yöneticisi: Doç.Dr.Lale ALATAN

Ortak Tez Yöneticisi: Prof. Dr. S.Sencer Koç

Haziran 2016, 79 Sayfa

GPS karıştırıcılar, GPS alıcılarına düşük güçte ulaşan GPS sinyallerinin üzerine fazladan gürültü ilave ederek alıcıların pozisyon verisi üretme hizmetini kısmen ya da tamamen devre dışı bırakırlar. GPS karıştırıcıların etkinliğinin giderilebilmesi için en popüler yöntem, anten dizisi ve dizi sinyal işleme yöntemlerinin kullanılması ile karıştırıcılarının uzaysal filtreleme ile bastırılmasıdır. Bu tez çalışması ile aktif anten tasarımı ve hüzme yönlendirme algoritmalarının kullanımı ile yukarıda bahsedildiği gibi GPS karıştırıcılarının uzaysal filtreleme ile bastırılması hedeflenmiştir. Bu tez çalışmasında, dört elemanlı aktif anten dizisi tasarımı, huzme yönlendirme algoritmalarının uygulaması ve gerçek zamanlı GPS karıştırıcı bastırma testleri olmak üzere üç ana başlık bulunmaktadır. Aktif anten dizisi tasarımı sırasında, öncelikle dairesel polarizasyona sahip yaklaşık kare tasarımlı mikroşerit anten tasarımı ve üretimi gerçekleştirilmiştir. Yöntemin geçerliliği görüldükten sonra aynı yöntemle dört elemanlı dairesel anten dizisi tasarım ve üretimi gerçekleştirilmiştir. Sonrasında ise anten dizisi ile kompakt bir dizayn oluşturacak şekilde dört kanallı düşük gürültülü yükselteç kartının tasarım ve üretimi gerçekleştirilmiştir. Huzme yönlendirme bölümünde, Capon huzme yönlendirme ve sıfır kazanç yönlendirme şeklinde iki ana huzme yönlendirme algoritmasının teorisine ve MATLAB ortamındaki simülasyon sonuçlarına yer verilmiştir. Bütün sistemin GPS karıştırıcı bastırma performansı, gerçek GPS uydularının ve gerçek karıştırıcı kaynağının kullanıldığı senaryo ile ispat edilmiştir.

ANAHTAR KELİMELER: Yaklaşık Kare Mikroşerit Anten, Dairesel Polarizasyon, Anten Dizisi, Huzme Yönlendirme, GPS Karıştırıcı Bastırma

To My Family and My Love

ACKNOWLEDGEMENTS

I would like to express my sincere appreciation to my advisor Assoc.Prof.Dr.Lale Alatan because she has enlightened me during all of my work, guided me with her higher patience and provided to keep my motivation at higher level.

I would like to express my sincere gratitude to my co-advisor Prof.Dr.S.Sencer Koç for his big effort during antenna measurements and valuable advices about my work.

I would like to thank to employees of electromagnetic laboratory, Erdinç Yurdakul and Adem Ateş for their big help during antenna production processes.

I would like to thank to my company, HAVELSAN Inc., for their all support and provide me opportunity to finish this thesis work.

I would also like to express my appreciation to my director in HAVELSAN Inc., Dr.Tolga Sönmez, because he supported me in all the period of this thesis work and guided me. In addition to that, I appreciated to my colleague Fatih Erdem for his help and support whenever needed, particularly in preparation of test setup and implementation of real time GPS antijamming scenarios.

My deepest gratefulness goes to my family who have the biggest effort on the point where I have arrived today and has right on all of my achievements in my life.

TABLE OF CONTENTS

LIST OF TABLES

TABLES

LIST OF FIGURES

FIGURES

LIST OF ABBREVIATIONS

GPS	:	Global Positioning System
C/A Code	:	Coarse/Acquisition Code
P(Y) Code	:	Precision Code
J/S	:	Jammer to Signal
INS	:	Inertial Navigation System
LNA	:	Low Noise Amplifier
GAJT	:	GPS Anti-Jamming Technology
DIGAR	:	Digital Integrated GPS Anti-jam Receiver
SAS	:	Small Antenna System
SNR	:	Signal to Noise Ratio
SINR	:	Signal to Interference and Noise Ratio
GNSS	:	Global Navigation Satellite Systems
CST MS	:	Computer Simulation Technology Microwave Studio
MUSIC	:	Multiple Signal Classification
CW	:	Continuous Wave
CP	:	Circular Polarization
EP	:	Elliptical Polarization
LP	:	Linear Polarization
RHCP	:	Left Hand Circular Polarization
LHCP	:	Right Hand Circular Polarization
VSWR	:	Voltage Standing Wave Ratio
AR	:	Axial Ratio
AF	:	Array Factor
UCA	:	Uniform Circular Array
VNA	:	Vector Network Analyzer
IC	:	Integrated Circuit
DOA	:	Direction of Arrival

CHAPTER 1

INTRODUCTION

GPS is the first comprehensive satellite based navigation system in the world. GPS program has started in 1973 by USA. It has become fully operational in 1993 with functional 24 satellites in 6 orbits. Altitudes of satellites are around 20000 km. The position finding concept of GPS is based on triangulation [1] method that uses distance measurements from reference point to some known positions in space. Triangulation method is visualized in Figure 1-1 in two dimensional space. For the point that we want to find the position on earth, there are three basic unknown position parameters that are x, y and z. Since there are three basic unknown parameters, positions of at least three satellites should be known. The basic position finding concept by using GPS satellites is shown in Figure 1-2. The satellites have atomic clocks that are continuously synchronized but the receiver does not have such an advanced clock. So the bias in the receiver clock is regarded as an unknown. Consequently, a GPS receiver needs to receive signals from at least 4 satellites for accurate positioning.

GPS signals are transmitted in two frequency bands. GPS L1 band is centered at 1575.42 MHz and GPS L2 band is centered at 1227.60 MHz. GPS signals are composed of three parts that are carrier wave, navigation data and spreading sequence. Carrier waves are created in center frequencies of L1 band and L2 band. Navigation data have a bit rate of 50 bps and includes information about the satellites orbit. The navigation data is coded by using two different types of codes associated with each satellite in order to benefit from the virtues of spread spectrum techniques. These codes are coarse acquisition code (C/A) and encrypted precision code (P(Y)). C/A code which is available for both civilian and military users has 1.023 MHz bit rate and uses 2.046 MHz bandwidth in only GPS L1 band.

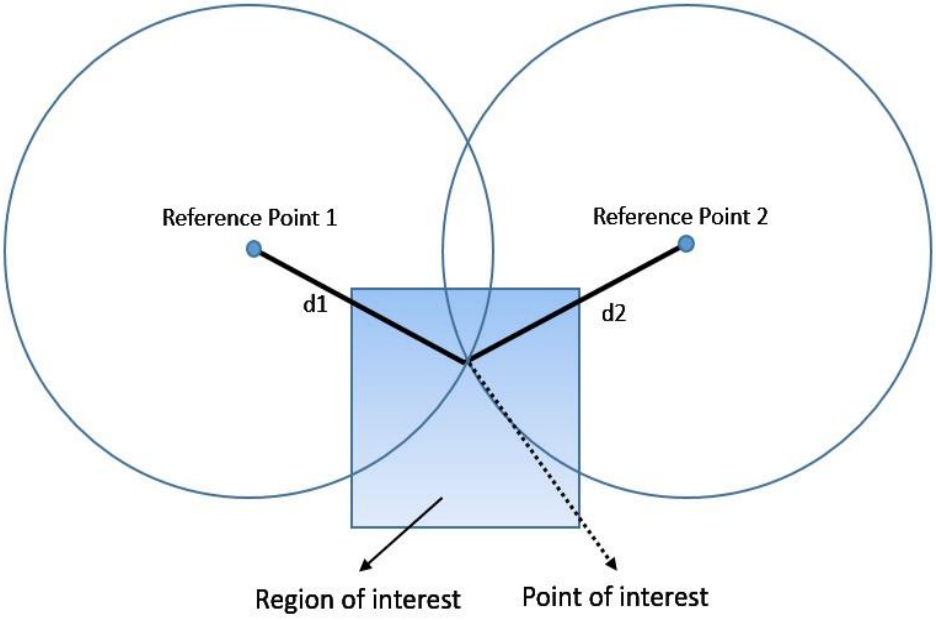

Figure 1-1 Triangulation in 2D space by using distance measurements d1 and d2 from two reference points

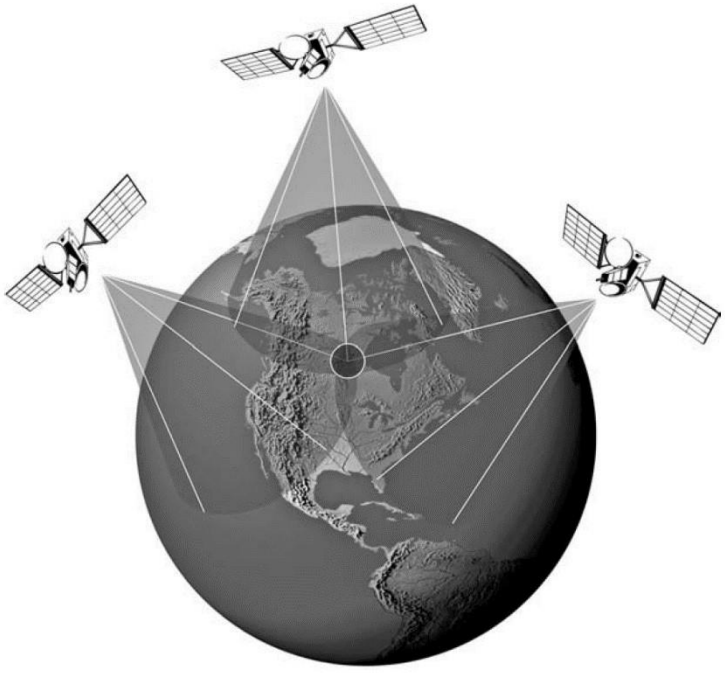

Figure 1-2 Triangulation for position finding with GPS satellites[1]

P(Y) code which is available for military users has 10.23 MHz bit rate and uses 20.46 MHz bandwidth in both GPS L1 and L2 bands. The GPS signal is modulated by Binary Phase Shift Keying (BPSK) method [2] as shown in Figure 1-3.

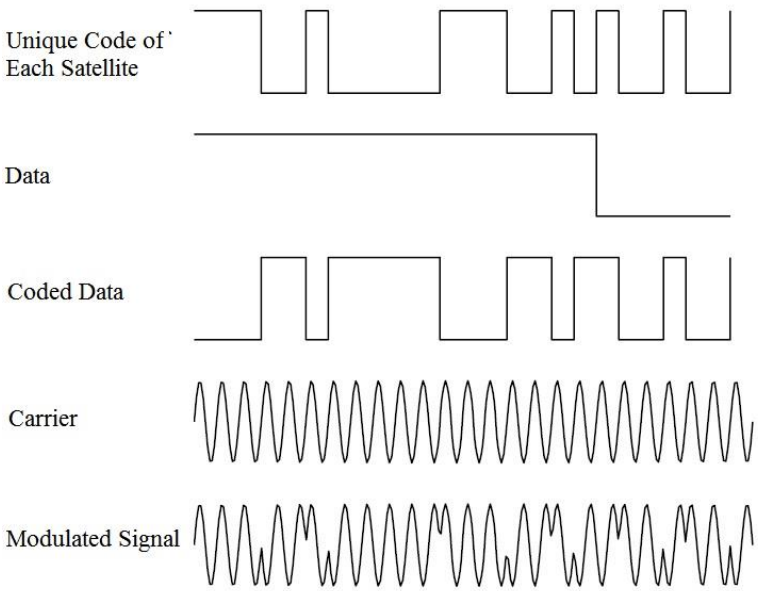

Figure 1-3 Effect of BPSK on the signal Structure for one antenna [2]

GPS satellites are orbiting at an altitude of about 20000 km. Because of such a large distance between satellite and receivers, GPS signals arrive receivers at very low power levels. The power level of GPS signal on earth is nearly -164 dBW. The GPS receiver can retrieve the navigation data from this low level signal by using the correlation of it with the code of satellite. However, when a jammer is present in the neighborhood of the GPS receiver, the acquisition of satellites may not be possible and it may interrupt the positioning service. There are two different operational modes for C/A code. These are acquisition and tracking modes. To make the acquisition faster, only a section of the code is used during the acquisition mode. Hence the code gain of this mode is smaller compared to tracking mode. Consequently C/A acquisition mode is more vulnerable to noise and interference so it may be lost at lower jammer to signal (J/S) ratios. In Figure 1-4, the change in J/S ratio according to distance between jammer and receiver is presented. Jammer power according to previously given GPS signal power represents in-band jammer power for GPS L1 band width. GPS signal power S is taken as -131 dBm. In this figure, C/A acquisition level (~25dB) refers to

the J/S ratio below which acquisition is not possible. Whereas below C/A loss level (~46 dB), the operation in the tracking mode is lost. It is understood from the figure that the acquisition of C/A code is prevented with even a 10-milliwatt jammer from 10 kilometers. These data show the ease of intentional or unintentional jamming on GPS receivers to interfere positioning service. Since in both civilian and military area the dependence on navigation systems such as GPS is increasing day by day, GPS jamming becomes a more important problem to be solved.

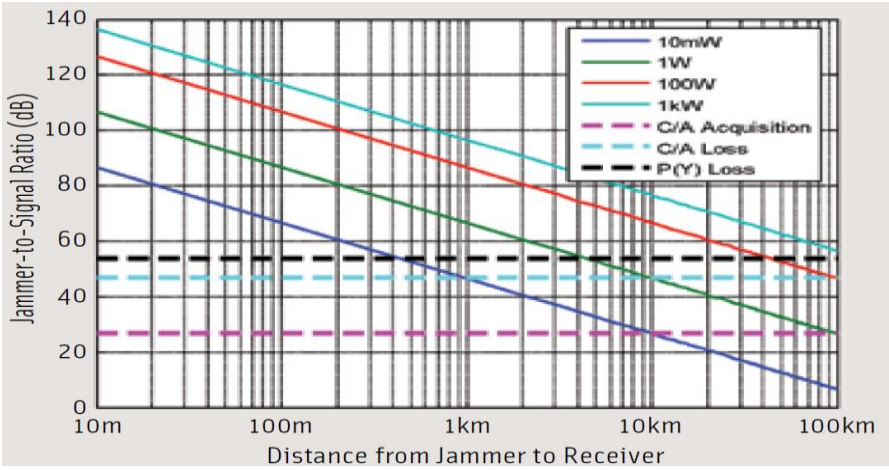

Figure 1-4 Effect of various jammers on GPS receiver [3]

In the market, there are many hand held GPS jammers that can be easily obtained [4]. In addition to that, there are some high power jammers that can be achieved only under some military regulations. Due to increasing popularity of jamming threat with the purposes such as personal privacy, terrorism and electronic warfare, researchers are actively working on the solution techniques to overcome jamming problem on navigation systems for both military and civilian users. The most commonly used methods that are summarized in [5] are notch filtering for continuous wave jammers [6], design of multi frequency multi system (GPS, GLONASS, GALILEO) receivers [7] and antenna arrays with controllable radiation pattern based solutions [8]. In addition to these, some sensors such as Inertial Navigation System (INS) can be used to increase accuracy of GPS positioning. Among these approaches, there are more efforts on spatial suppression of jammers by using antenna arrays with controllable null regions in their radiation patterns. Because long term GPS availability is possible

with this way and there is no need for any other navigation system like GLONASS or GALILEO. There are some good examples of commercially available GPS anti-jamming systems based on spatial suppression of jammer sources. GAJT of Novatel-Qinetic[9], DIGAR of Rockwell Collins[10], TopShield of Thales[11] and SAS of BAE Systems[12] can be counted as the most important products in this area. These systems are generally designed using arrays with 4 or 7 antenna systems.

The aim of this thesis is to construct a jammer protection system for civilian GPS receivers by designing an active antenna array and implementing a beam-forming algorithm to adaptively and automatically control the pattern of this array according to the position of the jammer. The number of array elements are chosen as 4. Although larger number of elements improves the jammer suppression performance of the system, 4 elements are evaluated to be sufficient to demonstrate the main concept. Active antenna array unit is composed of an antenna array and a Low Noise Amplifier (LNA) for each element and this LNAs are used to amplify low level GPS signals. The output of each LNA is converted to Intermediate Frequency (IF) band from Radio Frequency (RF) band, then they are digitized and sent to the beamforming algorithm. The output of the beamforming algorithm is the complex weighting coefficients for each element. Finally, the output of the array is converted to analog and up-converted back to RF band in order to be utilized by any commercially available GPS receiver. The block diagram of the overall anti-jamming system can be seen in Figure 1-5.

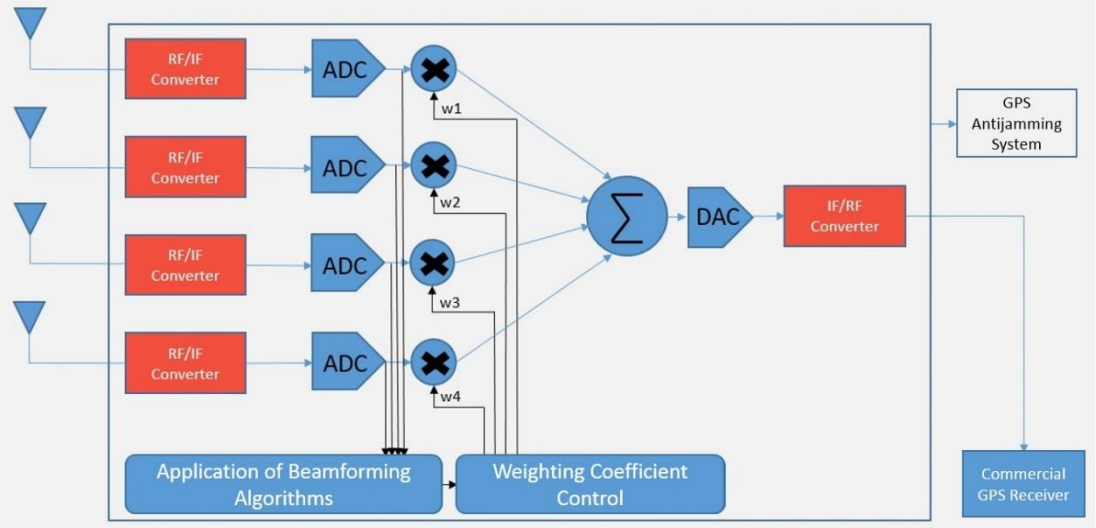

Figure 1-5 Overall block diagram of GPS anti-jamming system

In this thesis work, Chapter 2 gives information about specifications of GPS antennas and some GPS antenna types available in the literature. In this thesis, nearly square micro-strip patch antennas are chosen as the array elements. After reviewing the basic concepts of micro-strip antennas, the design procedure proposed in this thesis for the design of nearly square micro-strip patch antenna will be presented. The electromagnetic simulations of the antenna is performed by CST Microwave Studio [13] and the parameters of the designed antenna are further optimized through a couple electromagnetic simulations. The optimized antennas with different substrate heights are manufactured and measured. The measurement results and simulations of the antennas are compared in this chapter.

Chapter 3 provides information about the 4 element active antenna array design. The designed four element antenna array is manufactured and measurements are performed. The effect of mutual coupling on the radiation pattern of the antenna array is discussed here. The information about four channel LNA card is also provided in this chapter.

Chapter 4 is devoted to beamforming algorithms that aims to steer null in the direction of arrival of the jammer. There are two main classes that include the beamforming algorithms. These are blind (Eigen Decomposition-Based Subspace Technique, Multiple Independent Conventional Beamformers) and non-blind (Null Steering, Capon, Minimum Mean Square Error, MaxSINR (Signal to interference plus noise ratio), Sampled Matrix Inversion) techniques [14]. While non-blind algorithms use only the direction of arrival of the target signal or reference of the incoming signal, blind algorithms also utilize a priori information like the direction of arrival of the jammer and signal of interest. In this thesis, two beamforming approaches are implemented. One of the approaches is the Capon beamforming method and classified as a non-blind algorithms. For this method, only incoming direction of the target signal is needed and it is gathered from the almanac data of the GPS system. The other approach can be classified as a blind algorithm and includes direction finding of jammer sources with one of the direction finding algorithms (Conventional Beamforming, MUSIC (Multiple Signal Classification), ESPRIT) [15] and application of null steering through these directions. The incoming direction of the target signal is gathered from almanac data again. In application of this approach, Multiple Signal Classification (MUSIC) algorithm is used for direction finding purposes. In Chapter

4, Capon beamforming algorithm and application of both direction finding by MUSIC method and null steering algorithm are summarized. Then simulation results obtained through two different codes developed in MATLAB [16] environment are presented and compared for these two approaches.

Chapter 5 presents measurement results obtained with manufactured active GPS antenna array and CW jammers.

Chapter 6 concludes my thesis with overall comments on my work and possible future works to proceed my work.

CHAPTER 2

GPS ANTENNA DESIGN

Since the GPS antenna will be designed for C/A code, it will operate at L1 band which is centered at 1575.42 MHz with 2.046 MHz bandwidth. Frequency characteristics of the antenna should be designed according to these center frequency and bandwidth requirements. An input return loss characteristic with a narrow bandwidth helps to eliminate interference signals outside the GPS bands. One of the important requirements of GPS antennas is to provide signal reception for all look angles at the given signal to noise ratio of the receiver. To achieve uniform coverage of all satellites, a radiation pattern with a broad lobe over the upper hemisphere (beam width $\geq 130^{o}$) is required and the maximum variation over the main beam should be limited by 6dB. In addition to these, polarization is another important concern while designing GPS antenna. For the wave that is propagating in a space, wave polarization is the property that describes its electric field rotation at a fixed point as a function of time. Existing of same polarization types between receiving and transmitting antennas make possible to take transmitted signal by receiver without any loss [17]. There are three types of polarization that are linearly polarized (LP), elliptically polarized (EP) or circularly polarized (CP). GPS signals are Right Hand Circularly Polarized (RHCP) because of two main reasons. First of all, circularly polarized signal doesn't require correct alignment of receiver and transmitter antennas while LP and EP need correct alignment of these antennas. Secondly, CP is used to reject multipath signals. This rejection is due to the fact that the sense of polarization (right or left hand) reverses (RHCP to LHCP) when wave is reflected from ground. Hence the reflected multipath contribution cannot be received [18]. To sum up, a high rejection of cross-polarized signal (≥17dB) helps to discriminate between the direct and reflected signals.

Helical, spiral and microstrip patch antennas are widely used examples of circularly polarized antennas. From these design types, microstrip patch antennas are

generally preferred in GPS receiver applications since they are low profile, conformable to planar and non-planar surfaces and simple and inexpensive to manufacture. In addition to these, their resonant frequency, polarization, pattern, and impedance can be easily tailored according to the design needs by modifying the shape of the patch [19]. In this chapter, the theoretical information about microstrip patch antenna is presented in the first section. Then the design procedure for nearly square microstrip patch antenna is outlined. After that, design of GPS L1 band antenna with nearly square patch is given with comparison of simulation and measurement results. This section is ended with sensitivity analysis of antenna's performance according to changes in design parameters.

2.1 Microstrip Patch Antenna

Microstrip antenna is composed of four main parts that are metallic patch, dielectric substrate, ground plane and feeding structure. The basic structure of microstrip antenna is shown in Figure 2-1. Microstrip antenna with different patch shapes as shown in Figure 2-2 can be preferred according to necessities in design. From these shapes; square, circular and rectangular are the most popular choices because of easiness in analysis and fabrication with attractive radiation properties [19].

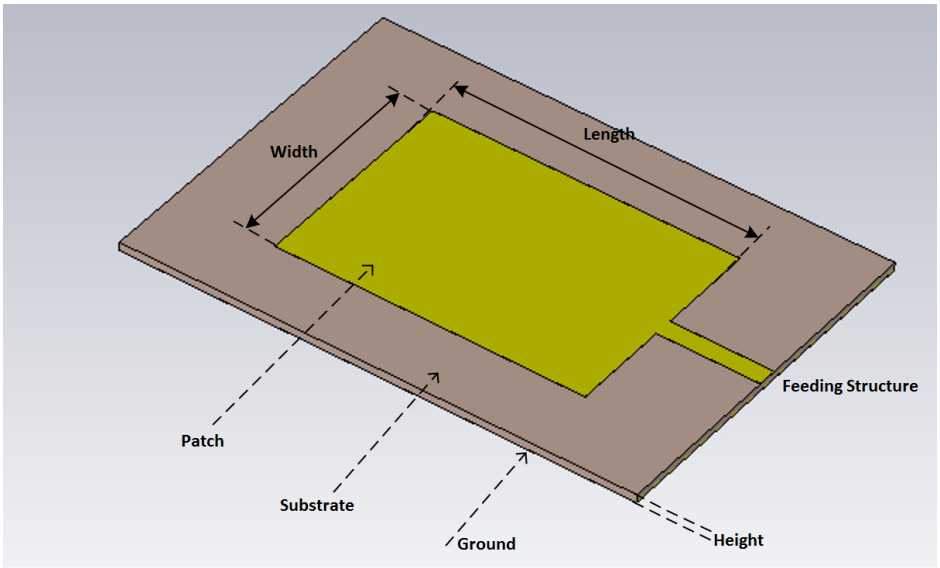

Figure 2-1 Microstrip antenna structure

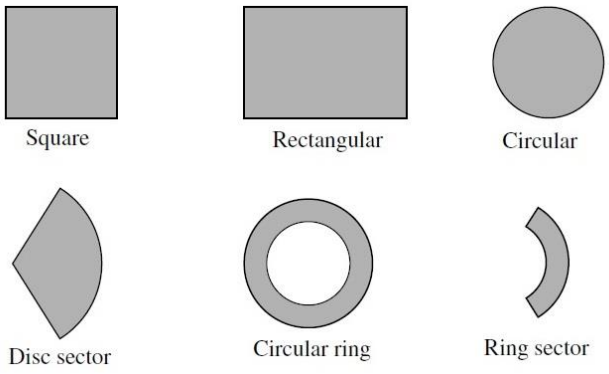

Figure 2-2 Microstrip antenna shapes [19]

Dielectric constant, loss tangent and height of the dielectric substrate are very important parameters while designing microstrip antennas. Dielectric materials that have dielectric constant ε_r between 2.2 and 12 is used generally. Designing a microstrip antenna that has high efficiency and bandwidth is possible by using thicker dielectric materials that has lower ε_r. Whereas, thin dielectric materials with higher ε_r is preferred for microwave circuits.

Another important issue during microstrip patch antenna design is the choice of feeding structure. There are four popular feeding structures that are coaxial feeding, microstrip line feeding, proximity coupled feeding and aperture coupled feeding. In this work, coaxial feeding is preferred in microstrip antenna design because of its simple design, easiness in fabrication, matching performance and low spurious radiation [19][20]. Figure 2-3 shows the structure of coaxial feeding in microstrip antenna design.

In the analysis of microstrip antennas either full-wave numerical techniques or approximate analytical methods can be used. While numerical methods provide high accuracy with a corresponding high computational cost, analytical methods offer fast and efficient estimation of antenna parameters for an initial design. Hence in this thesis, the initial parameters of the antenna are predicted by utilizing analytical methods, then they are fine-tuned by performing full wave analysis with commercially available electromagnetic simulation software.

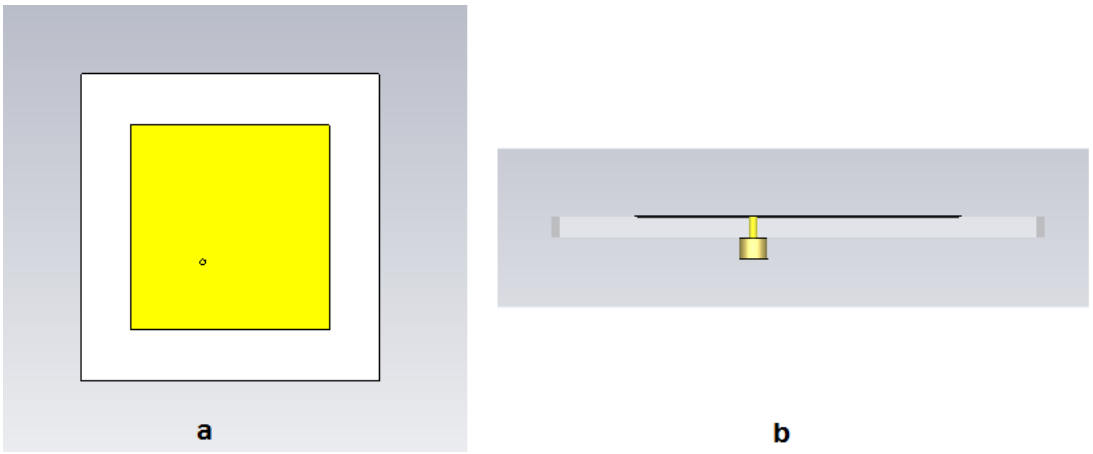

Figure 2-3 Coaxial feeding structure a) Antenna top view b) Antenna side view

There are two widely used analytical methods for the analysis of microstrip. One of them is transmission line model. It is the easiest analysis method for microstrip antennas. Although this model has lower accuracy and insufficiency to model coupling, it provides good physical insight. The other analytical method that provides physical insight is cavity model. It has higher accuracy but more complexity compared to transmission line model. In transmission line model, rectangular microstrip antenna can be represented by two slots separated by a transmission line of length *L*. Finite dimensions of patch along length and width result in fringing fields at the edges. Because of fringing, most of the electric field lines are placed in dielectric substrate while some of them are placed in air.

Fringing fields cause extension in physical dimensions of the antenna as shown in Figure *2-4*. The amount of length extension, ΔL, can be calculated by using the following empirical formula which is proposed in [21]

$$\Delta L = h \times 0.412 \times \frac{\varepsilon_{reff} + 0.3}{\varepsilon_{reff} - 0.258} \times \frac{\frac{W}{h} + 0.264}{\frac{W}{h} + 0.8} \tag{2.1}$$

where ε_{reff} is the effective dielectric constant of an equivalent homogeneous dielectric medium which can be substituted instead of the multilayered dielectric slab-air-mediums. ε_{reff} is calculated by using the following well-known expression [19]

$$\varepsilon_{reff} = \frac{\varepsilon_r + 1}{2} + \frac{\varepsilon_r - 1}{2}\left[1 + 12\frac{h}{W}\right]^{-\frac{1}{2}} \tag{2.2}$$

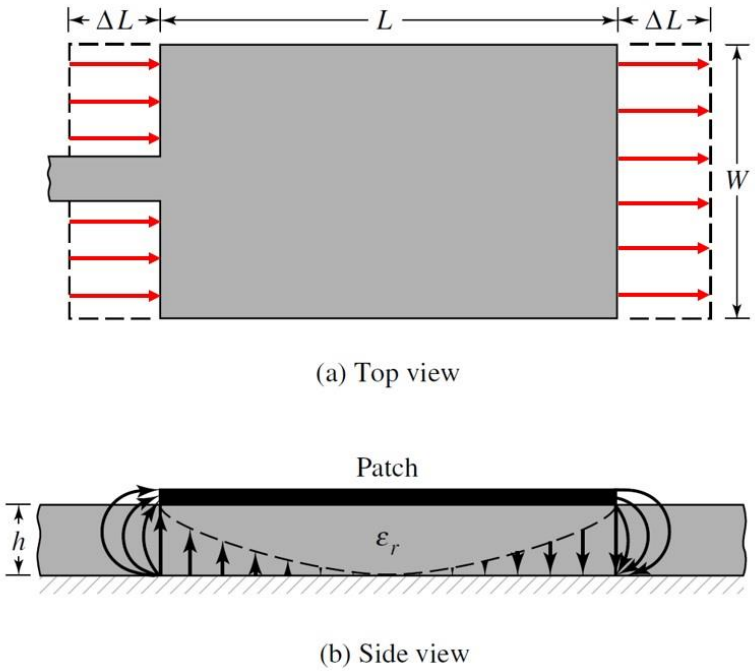

Figure 2-4 Fringing effect on patch antenna [19]

When the extended length of the patch *(L+2ΔL)* is equal to half guided wavelength, the antenna will be at resonance. Hence, the physical length of the patch is [19]

$$L = \frac{v_0}{2f_r\sqrt{\varepsilon_{reff}}} - 2\Delta L \tag{2.3}$$

where c and f_r represents the speed of light and resonant frequency of the microstrip antenna.

In cavity model, the patch antenna is modeled as a cavity with perfect electric conductors at the top and bottom surfaces (patch and ground plane) and perfect magnetic conductors on the side walls. Then the fields inside the cavity is solved by assuming that there are no field variations along the normal direction to the ground plane. This assumption is quite valid for electrically thin substrates. Infinitely many different modes can be excited inside the cavity but the dominant modes are TM_{010} and TM_{100} modes. The subscripts corresponds to field variations along x,y,z directions for a patch antenna situated at xy plane. When the patch is fed at the center of the edge along x(y) direction, only TM_{010} (TM_{100}) mode is excited.

Polarization is another very important concern of antennas as mentioned at the beginning of this chapter. Antennas can be classified as LP, EP and CP in accordance

with their polarization types shown in Figure *2-5*. Previously it is mentioned that GPS antennas should be RHCP. However, when the patch antenna is excited at the center of one of the edges, the antenna is LP. Therefore, some modifications on microstrip antennas are necessary to design circularly polarized antenna.

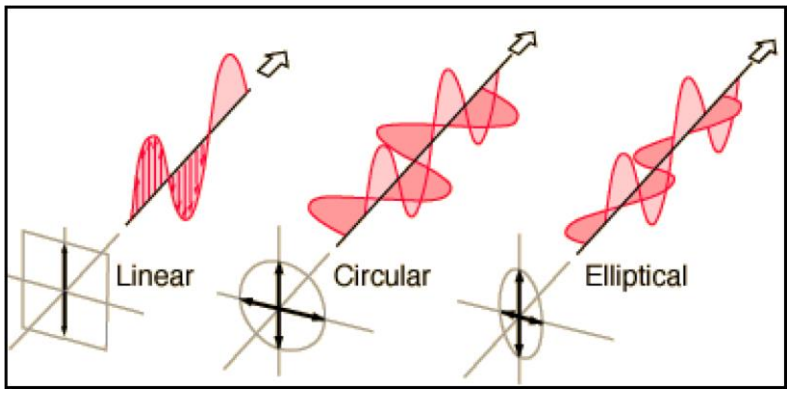

Figure 2-5 Polarization types [23]

Circular polarization can be achieved by exciting two orthogonal modes with 90^o phase difference and same amplitudes. If square patch antenna is considered, CP can be achieved by feeding the antenna from adjacent two edges. While one of the feeds is exciting TM_{010} mode, the other feed is exciting TM_{100} mode. The 90^o phase difference can be achieved either by using a power divider and a 90^o phase shifter as shown in Figure 2-6 or by using a 90^o hybrid coupler [19]. However this type of feeding is not suitable for array design due to limited space between antennas and increased mutual coupling effects.

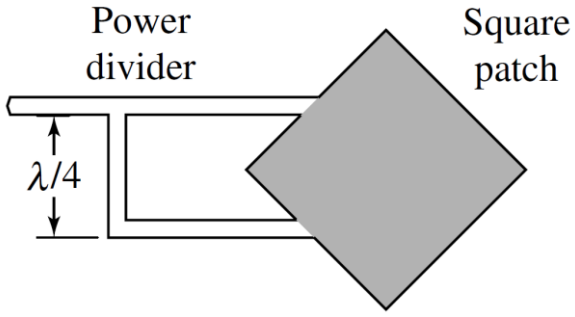

Figure 2-6 CP square patch antenna structure [18]

Circular polarization can also be obtained with single feed structure. To achieve this, two orthogonal modes should be excited simultaneously. 90° phase shift is obtained by utilizing the phase variation characteristics of the modes around the resonance frequency [24] When the resonance frequency of one of the modes (f_a) is slightly larger than operating frequency of the antenna (f_0) and resonance frequency of the other mode (f_b) is slightly smaller than f_0, the 90° phase shift is achieved as shown in Figure 2-7. Two common patch shapes for CP operation with single feed are nearly square patch and truncated patch as shown in Figure 2-8 (a) and (b) respectively. For nearly square patch, length and width of the patch are nearly the same that provide the necessary amplitude and phase relations between TM_{010} and TM_{100} modes [19]. In truncated patch two opposite corners are trimmed and the patch is fed at the center of one of the edges according to required polarization sense. In this work, nearly square patch is preferred because of its better cross polarization properties.

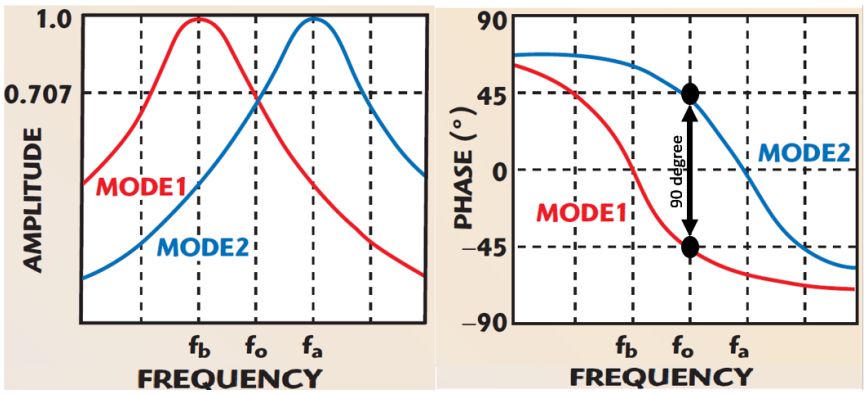

Figure 2-7 Amplitudes and Phases of Two Degenerate Modes [25]

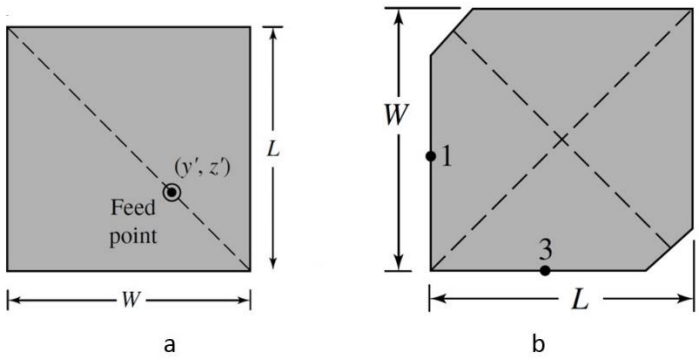

Figure 2-8 a) Nearly Square b) Truncated [19]

The performance parameter to measure the quality of CP is the axial ratio (AR) and AR levels below 3 dB is generally considered to be acceptable CP operation.

Nearly square microstrip patch antenna design begins by specifying substrate type, height of substrate and operating frequency. After decision of these parameters, patch dimensions needs to be estimated. In this thesis, nearly square patch antenna design is performed based on works presented in [26] and [27]. As it well known from circuit theory the sharpness of the amplitude variation curve and the slope of the variation curve of a resonator are related to the quality factor (Q) of the resonator. Hence f_b, f_0 and f_a are related to each other through the *Q* value of the antenna. Moreover W and L values determines f_a and f_b. Based on these observations [26], the W/L ratio is proposed to be equation (2.4)

$$\frac{W}{L} = \frac{2 \times Q + 1}{2 \times Q - 1} \tag{2.4}$$

Hence to estimate the *W/L* ratio one needs to know the *Q* value of the antenna. *Q* value of the microstrip antenna depends on the parameters of the substrate and the operating frequency. To predict the *Q* value of the chosen substrate at the design frequency, the bandwidth-Q value relations proposed in [27] are utilized. The input impedance percentage bandwidth of a LP antenna (BW_{LP}^{IMP}) for $VSWR_{max}$ (Voltage Standing Wave Ratio) is given as:

$$BW_{LP}^{IMP} = \frac{VSWR_{max} - 1}{\sqrt{VSWR_{max}} \times Q} \tag{2.5}$$

Generally input return loss values below -10 dB are considered to be a good match and this corresponds to $VSWR_{max}$=2. To calculate the *Q* value of the antenna, first a LP square antenna is designed by using transmission line model then this antenna is analyzed by using electromagnetic simulation software CST-Microwave Studio. The impedance bandwidth of this antenna is found from the simulation results and corresponding *Q* factor is calculated by using equation (2.5). Finally *W/L* ratio is calculated from equation (2.4).

After the initial length and width values for nearly square patch antenna are decided, antenna is analyzed through the CST simulations and antenna dimensions are fine tuned. The probe feed location where antenna matches with 50Ω is also very important

and it is found with parameter sweep property of CST MS. In [27], the following expressions for estimating the input impedance bandwidth and the axial ratio bandwidth of the CP antennas are proposed:

$$BW_{CP}^{IMP} = \frac{\sqrt{2 \times (VSWR_{max} - 1)}}{Q} \tag{2.6}$$

$$BW_{CP}^{AR} = \frac{AR_{max} - 1}{\sqrt{AR_{max}}Q} \tag{2.7}$$

The bandwidth values obtained from simulation results and calculated values from (2.6) and (2.7) are compared to explore the validity of the proposed equations in [27] for different heights of materials in next section.

2.2 Design of GPS L1 Band Antenna with Comparison of Simulation and Measurement Results

During this thesis work, nearly square patch antenna design was performed with different materials like FR4, RO4003 and TMM10 and different height of substrates. At the beginning, FR4 material is chosen due to its easy availability and low cost. However, when the antenna is manufactured and measured, it is observed that the resonance frequency of the antenna is 40 MHz above the target frequency. After some research, it is learnt that FR4 material is a low quality material and its dielectric constant can vary from one plate to the other. In addition to this, dielectric constant of this material may not be homogeneous for the same plate. Therefore, it has been decided to use a material with higher quality and stable dielectric constant. For that purpose RO4003 material from Rogers Corporation is chosen. In this part, the two designs performed with same RO4003 material but with different substrate heights are discussed. The design process, simulation and measurement results are presented in detail at the following subsections.

2.2.1 Nearly Square Patch Antenna Design with RO4003 (h=1.524 mm)

RO4003 is a dielectric material that is fabricated by Rogers Corporation. Maximum height of manufactured dielectric material is 1.524 mm. The dielectric constant of

RO4003 material is 3.55. The operating frequency for GPS L1 band is 1575.41 MHz. After decision of material, substrate height and operating frequency, linearly polarized square patch antenna is designed. Input return loss versus frequency plot of LP antenna is shown in Figure 2-9. Using 15.97 MHz 10dB impedance bandwidth in equation (2.5), Q value is calculated approximately as 70 and the relation between width and length is found through equation (2.4). Dimensions of LP and CP antennas are listed in Table 2-1. As mentioned before probe locations are determined by parameter sweep tool of CST MS.

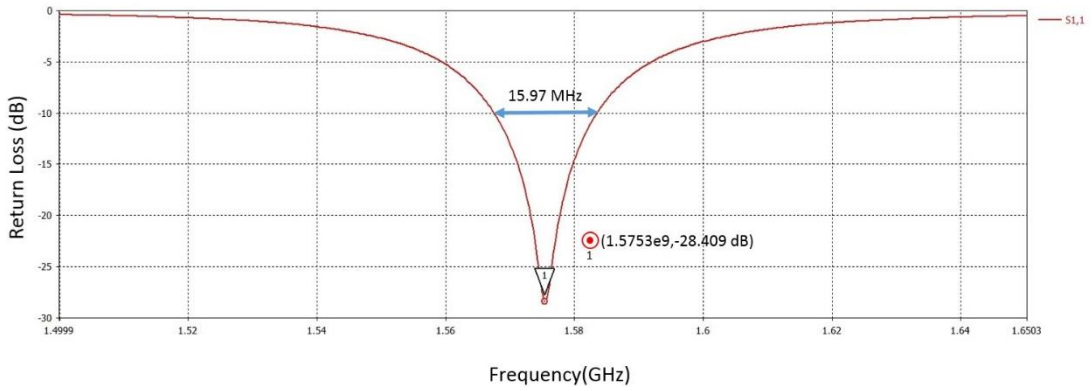

Figure 2-9 Return Loss of LP Antenna

Table 2-1 Dimensions of LP and CP Antenna

	LP	CP
Length	48.8 mm	48.5 mm
Width	48.8 mm	49.2 mm
Probe Location (Length Dir.)	19 mm	18 mm
Probe Location (Width Dir.)	19 mm	17 mm

As you can see from Table 2-1, the values of calculated dimensions and found values after fine tuning in CST are very similar that prove the accuracy of dimension estimation formulas that are given in equations (2.4), (2.5), (2.6) and (2.7).

The return loss plot of the CP designed antenna is shown in Figure 2-10. According to this figure, antenna is successfully matched to 50Ω and its operating frequency is proper for our purpose with 31.34 MHz 10 dB impedance bandwidth. According to AR plot that is shown in Figure 2-11, 3 dB AR bandwidth is larger than target bandwidth of GPS L1 band and antenna is proper to manufacturing according

to simulation results. It is very important to note that 3dB AR bandwidth region is inside the 10 dB impedance bandwidth. That means, antenna is CP in only some part of the radiation region.

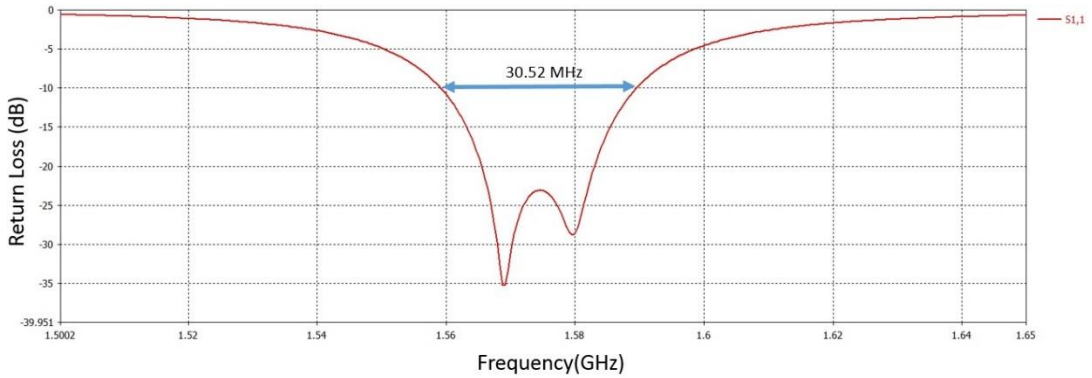

Figure 2-10 Return loss of CP antenna

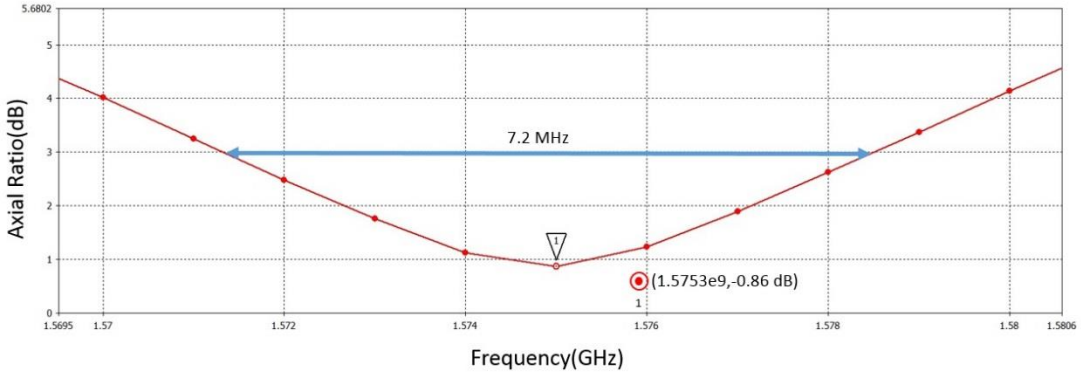

Figure 2-11 AR plot of CP antenna

3dB AR bandwidth and 10dB impedance bandwidth of simulated antenna are compared with calculated values obtained from equations (2.6) and (2.7) in Table 2-2. The results in this table demonstrates the accuracy of the relations proposed in [27].

Table 2-2 Comparison of calculated and simulated bandwidth values

	Calculation Results	Simulation Results
BW_{CP}^{IMP}	31.9 MHz	30.52 MHz
BW_{CP}^{AR}	7.85 MHz	7.2 MHz

Since the specifications are satisfied according to simulation results, the antenna is manufactured. Designed antenna was produced with LPKF ProtoMat H100 prototyping machine. After manufacturing, return loss of antenna was measured. According to measurement results, the center frequency of the antenna was at 1587 MHz. Because of the 12 MHz shift in the center frequency, tuning process is needed. According to sensitivity analysis performed and results presented in the following part of this chapter, antenna center frequency is tuned to target center frequency by increasing the length and the width of the antenna with copper band. The comparison of length and width of the patch before and after tuning is shared in Table 2-3. Top and bottom view of tuned antenna is shown in Figure 2-12. Comparison of return loss and AR results between simulation and measurement of tuned antenna are shown in Figure 2-13 and Figure 2-14.

Table 2-3 Comparison of patch dimensions before and after Tuning

	Before Tuning	After Tuning
Length	48.5 mm	49.3 mm
Width	49.2 mm	50 mm

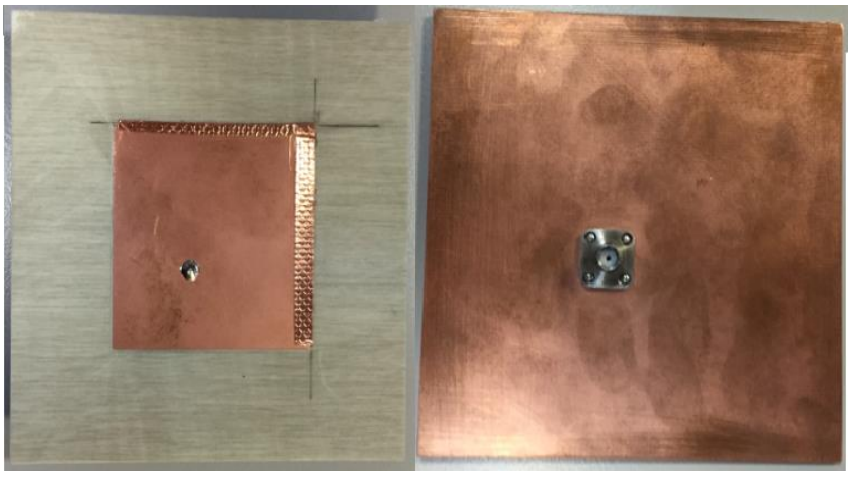

Figure 2-12 Top and bottom view of tuned antenna

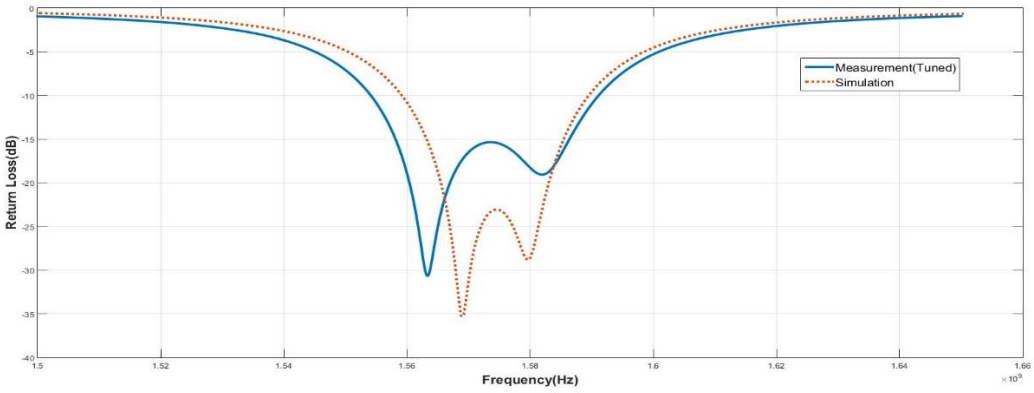

Figure 2-13 Comparison of return loss between simulated and manufactured antenna

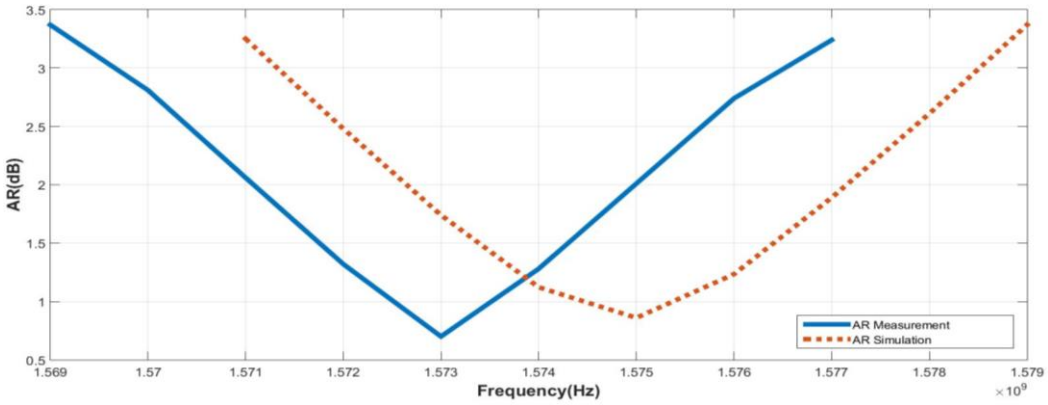

Figure 2-14 Comparison of AR between simulated and manufactured antenna

When this designed and tuned antenna is used in the array environment, the center frequency of AR bandwidth shifts more due to mutual coupling effects and the AR requirement within the target band cannot be achieved. One of the solutions for this problem is to design an antenna with larger bandwidth. An easy approach to increase the height of the substrate. The antenna design for h=3.048 mm is presented in the next subsection.

2.2.2 Nearly Square Patch Antenna Design with RO4003 (h=3.048 mm)

Because the availability of more RO4003 dielectric plate with h=1.524 mm, it is decided to press two plates with 1.524 mm height and obtain RO4003 plate with 3.048 mm height. First of all, linearly polarized antenna is designed and simulation results imply the 10 dB impedance bandwidth of the antenna is 30.6 MHz as shown in Figure 2-15. Using equation (2.5), the *Q* value of the antenna is calculated as 36.4. Recall that

the Q factor for h=1.524 mm was 70. Hence the Q factor is almost halved by doubling the height of the substrate. Using equation (2.4) dimensions of the patch are specified. The comparison of dimensions between LP and CP antennas and their feeding positions are given in Table 2-4.

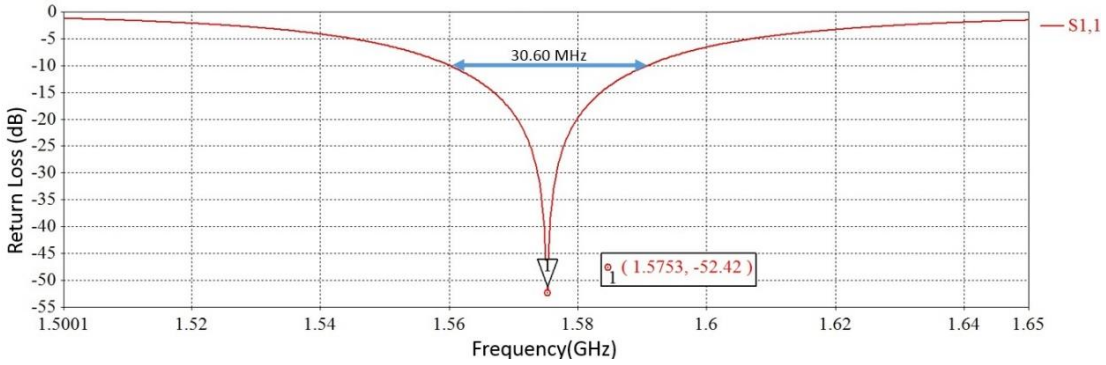

Figure 2-15 Return loss of LP antenna

Table 2-4 Dimensions of LP and CP antenna

	LP	CP
Length	47.71 mm	46.9 mm
Width	47.71 mm	48.3 mm
Probe Location (Length Dir.)	18.5 mm	17 mm
Probe Location (Width Dir.)	18.5 mm	16 mm

The importance of return loss measurement and axial ratio measurement was mentioned in the previous section. For the CP antenna with 3.048 mm substrate height, return loss and axial ratio simulation results are given in Figure 2-16 and Figure 2-17, respectively. 10 dB impedance bandwidth and 3dB axial ratio bandwidth of the simulated antenna are compared with the bandwidth values that are calculated according to equations (2.6) and (2.7) in Table 2-5. As it can be seen from the table, calculated and simulated values are close to each other. This comparison shows that the expression proposed in [27] are also valid for thick substrates.

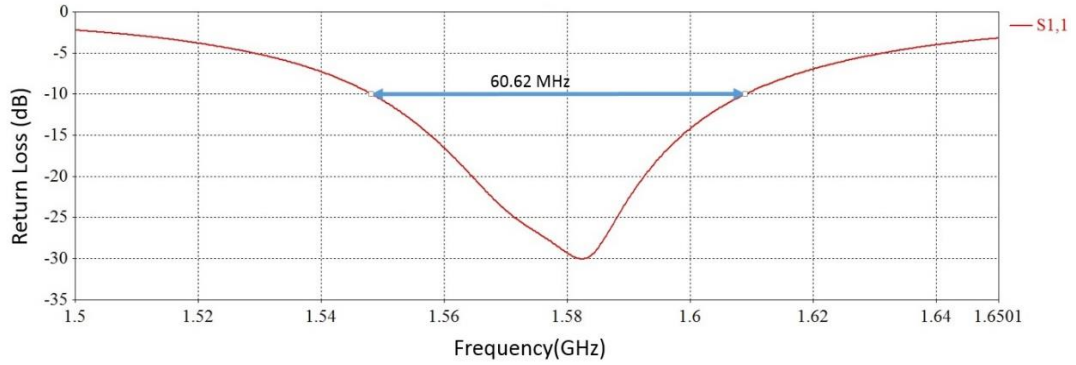

Figure 2-16 Return loss of CP antenna (RO4003 with 3.048mm height)

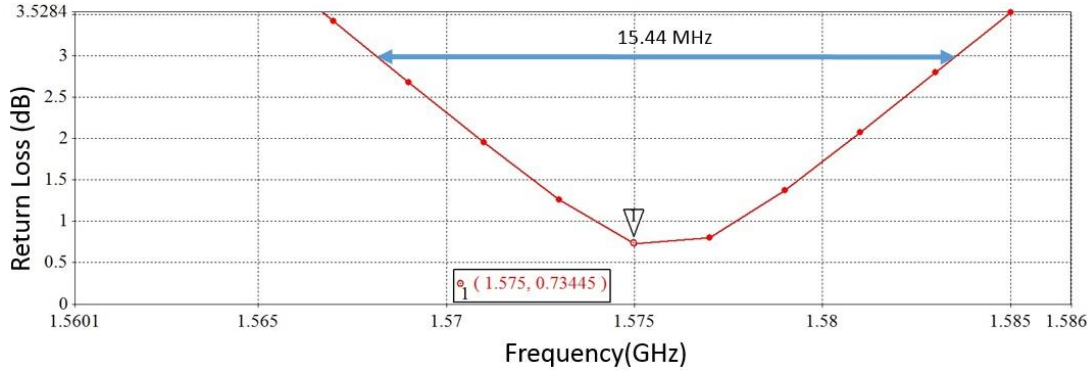

Figure 2-17 AR plot of CP antenna (RO4003 with 3.048mm height)

Table 2-5 Comparison of calculated and simulated bandwidth values

	Calculation Results	Simulation Results
BW_{CP}^{IMP}	61.2 MHz	60.62 MHz
BW_{CP}^{AR}	15.07 MHz	15.44 MHz

Note that the simulated 10dB CP impedance bandwidth and 3dB CP axial ratio bandwidths for the antenna with h=1.524 mm are 30.52 MHz and 7.2 MHz. For the antenna with h=3.048 mm, these values are 60.62 MHz and 15.44 MHz that are nearly double of the previous values. This is because of the relations between bandwidth values and Q factor. Since Q value of the antenna is halved, such an increase in bandwidths is an expectation.

RO4003 dielectric materials are produced with maximum 1.524 mm dielectric height. In order to get higher dielectric substrate, we used two pieces of RO4003 plates with

1.524 mm and press them with LPKF machine. During press process, 0.1 mm thick FR4 prepreg material is used between two materials. After press process is finished, RO4003 material with new substrate height was ready. Then, the production is performed with the parameters given in Table 2-4. In return loss and axial ratio measurements of the manufactured antenna, nearly 16 MHz shift in center frequency is observed although the bandwidth measurements are almost same with the simulated one. In order to tune this antenna, the necessary shifts in length and width of the patch are calculated and applied in simulation program. Then, antenna is remanufactured with this updated dimensions. After manufacturing of this tuned antenna, the return loss and axial ratio measurements are performed. The return loss comparison of simulation and measurement results for the manufactured antennas is shown in Figure 2-18. As shown in this figure, the firstly manufactured antenna has shifted center frequency with good matching property. After remanufacturing with tuned dimensions, the antenna has nearly same return loss properties with the simulated one.

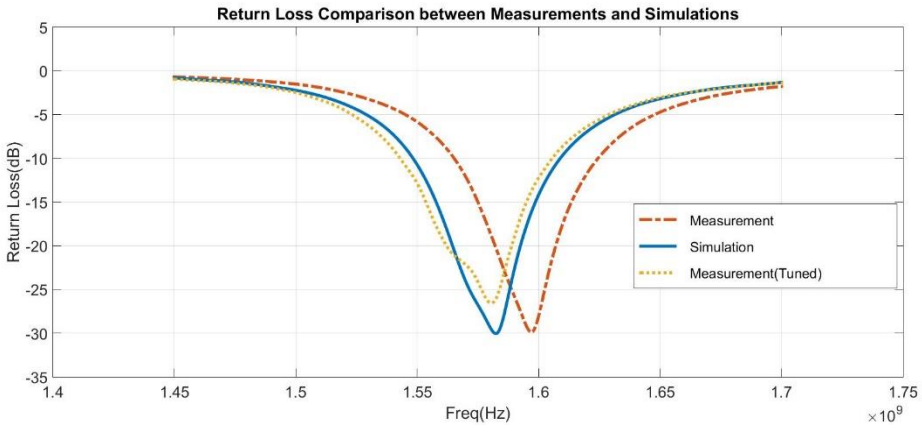

Figure 2-18 Return Loss Comparison between Simulations and Measurements

For circularly polarized antennas, AR characteristics are more important than return loss variations. AR comparison of simulation and measurement results for the manufactured antennas is shown in Figure 2-19. From AR measurements of the manufactured antennas, it can be said that the shift in the target center frequency of the antenna is disappeared with tuned antenna. The 10 dB impedance and 3 dB axial ratio bandwidth of the manufactured antenna is compared with the simulated one in Table 2-6. Although the center frequency of the tuned antenna is not at the target center

frequency, the 3dB AR bandwidth includes the bandwidth for the civilian users at GPS L1 band.

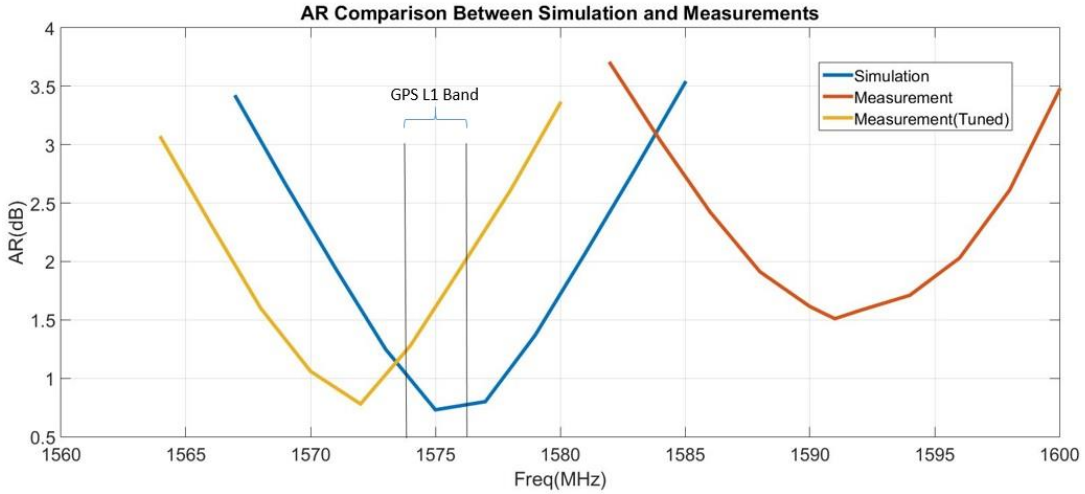

Figure 2-19 AR Comparison between simulation and measurements

Table 2-6 Bandwidth comparison between simulation and measurement results

	Measurement Results	Simulation Results
BW_{CP}^{IMP}	59.5 MHz	60.52 MHz
BW_{CP}^{AR}	15 MHz	15.44 MHz

After return loss and axial ratio measurements, radiation pattern of the tuned antenna is measured. Under transmission of RHCP and LHCP signals at 1575 MHz, the radiation pattern comparison for the first principle plane is shown in Figure 2-20. According to this measurement, this antenna has around 20 dB cross polarization rejection rate and above 25 dB front to back ratio. 3dB beamwidth of the antenna is above 105º. Cross polarization rejection and front to back ratio is very good for the usage in GPS application. Although 3dB beamwidth is slightly smaller than the target 3dB beamwidth, this is not an obstacle to use this antenna as a GPS antenna.

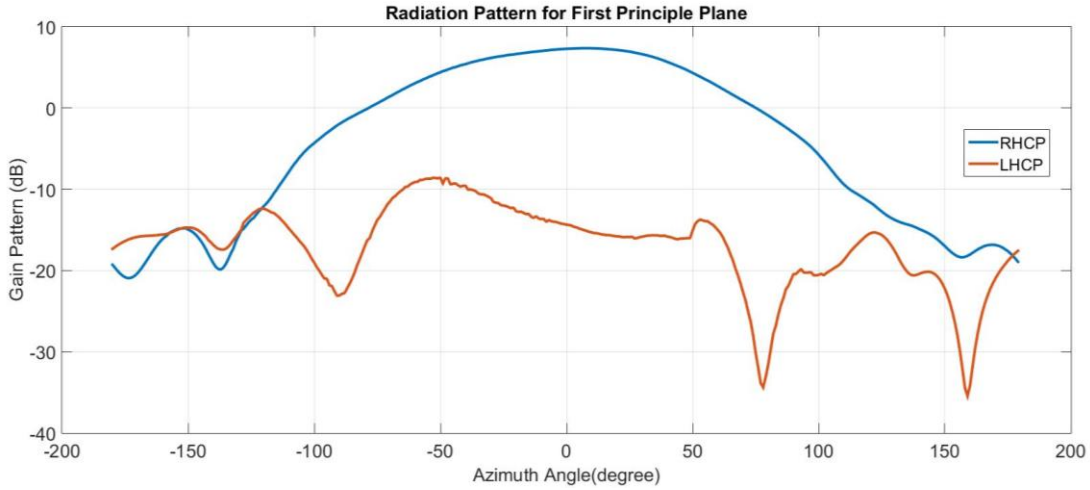

Figure 2-20 Radiation pattern of the antenna for first principal plane

2.3 Sensitivity Analysis According to Changes in Antenna Parameters

In order to get better insight about the effect of small changes in antenna parameters on the antenna performance, sensitivity analysis of CP antenna is performed. During the sensitivity analysis, the effects of changes in the length of the patch, size of the ground plane, the location of probe and dielectric constant of the substrate on the antenna performance are observed. These analysis help to interpret the differences between simulation and measurement results. Also they guide the antenna designer during the tuning phase of the manufactured antenna. The sensitivity analysis are performed by using parameter sweep property of CST MS electromagnetic simulation tool. For evaluation of the changes in parameters, the CP nearly square antenna that is presented in section 2.2.1 is considered as reference.

2.3.1 Changing Length of the Patch

Length and width of the patch antenna are very important parameters that specify the radiation properties of the antenna and circular polarization. According to equation (2.3), the length or width of the antenna is inversely proportional with frequency. In other words, if the length, width or both of them for the manufactured antenna are higher than the dimensions in simulations, the operating frequency of the antenna decreases. If there is change only in length of the patch, the center frequency of the corresponding mode changes and the circular polarization property of the antenna can be lost and W/L ratio is disturbed.

Sensitivity analysis for length of the patch was performed changing the dimension from 48.1 mm to 48.8 mm with 0.1 mm steps. The real value of length is 48.5 mm. The change of return loss measurements according to change in length is given in Figure 2-21. In addition to this, the change in axial ratio according to change in length is given in Figure 2-22. Since length is the smaller dimension and width is the larger dimension of the antenna, the lower resonance is determined by the width and the higher resonance is determined by the length of the antenna. Consequently as it can be observed from Figure 2-21, the changes in the length slightly affect the lower resonance while it considerably shifts the higher resonance. From Figure 2-22, it is understood that the polarization property of the antenna is directly affected by the change in length as discussed above. CP operation is possible only for a restricted range of W/L ratios. From both return loss and axial ratio measurements according to change in length, it can be concluded that any manufacturing error above 0.1 mm in length or width can prevent the achievement of desired antenna properties. Another result that can be concluded from these figures is that, if the measured center frequency of the manufactured antenna is different from target center frequency, the target center frequency can be achieved by tuning the length or the width of the patch antenna.

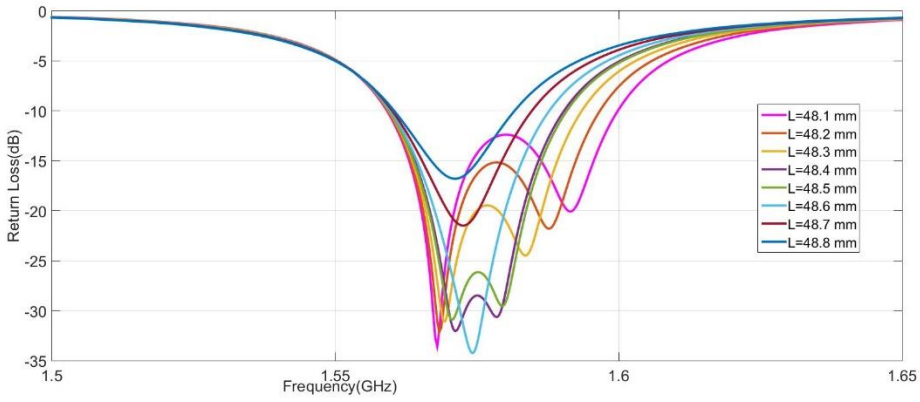

Figure 2-21 Return loss change for various length dimensions

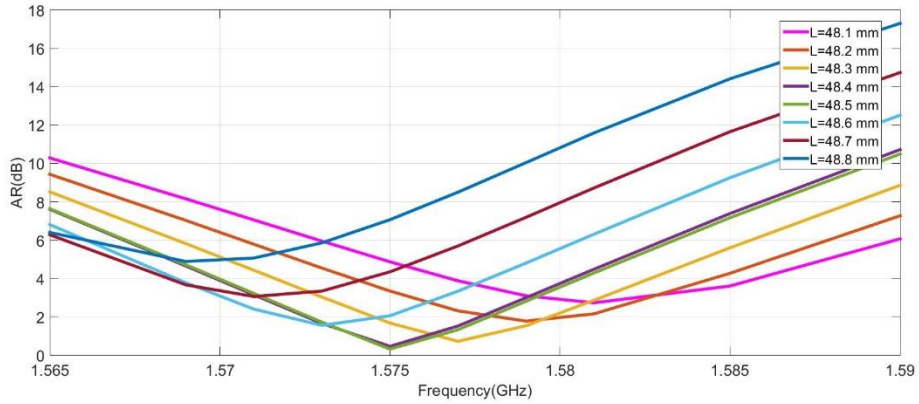

Figure 2-22 Axial ratio change for various length dimensions

2.3.2 Sliding the Feed Point of the Antenna

Feed location of the patch antenna is also very important in order to get desired radiation properties. Therefore, the effects of possible shifts in feed location on the radiation performance of the antenna is studied. For the antenna that is mentioned in section 2.2.1, the feeding point is 18 mm far away from left bottom corner in x direction and 17 mm in y direction. For the sensitivity analysis, the feed location is swept between from 17.4 mm and 18.6 mm in x direction. According to return loss simulation results that are given in Figure 2-23, the change of feed location can seriously change the radiation properties of the antenna. The feed location mainly determines the amplitudes of the two orthogonal modes. These modes have almost same amplitudes as long as the feed remains on the diagonal.

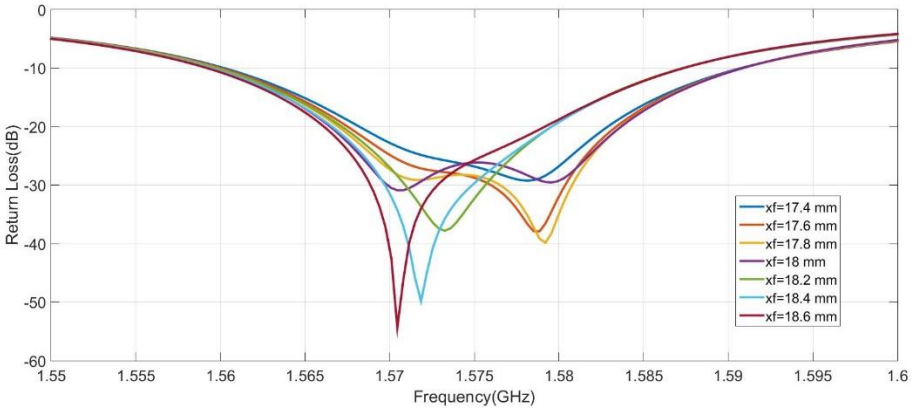

Figure 2-23 Return loss change for different feed locations

As the feed diverts from the diagonal, one of the modes is excited more dominantly and circular polarization may not exist. This result can be verified also examining Figure 2-24. In conclusion, the shift in the feed location can be the potential cause of the differences in the antenna performances for the simulation and measurement results.

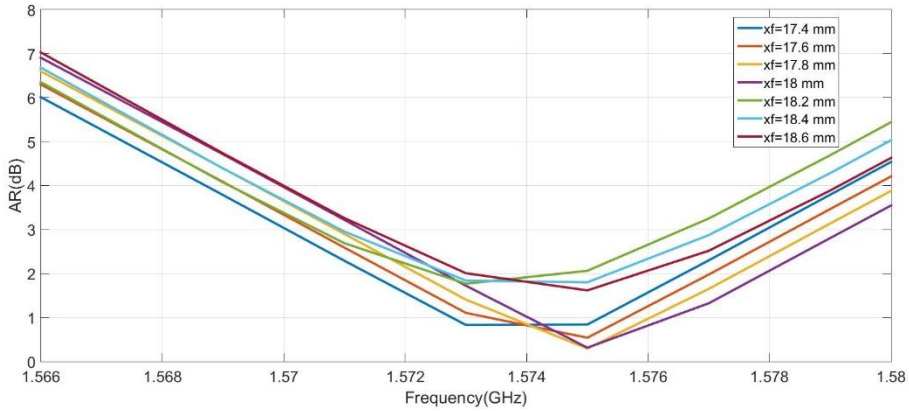

Figure 2-24 Axial ratio change for different feed locations

2.3.3 The Effect of Changes in Dielectric Constant on the Antenna Performance

Dielectric constants of dielectric materials are varying with change in operating frequency. In addition to this, dielectric constants of some materials may change from one sample to other sample according to production quality of the material. For RO4003C material, the dielectric constant for the design is reported as 3.55. For the sensitivity analysis, dielectric constant ε_r of dielectric material is varied between 3.4 and 3.7 with 0.05 steps. The return loss results and axial ratio results are given in Figure 2-25 and Figure 2-26, respectively. It can be observed that the dielectric constant directly affects the center frequency. More explicitly, if the dielectric constant of the material used in manufacturing is higher than the value that is used in simulation, the measured center frequency of the antenna will be smaller than the simulation results. Another interesting observation is that the circular polarization of the antenna does not change but CP operation occurs at different frequency. This is due to the fact that dielectric constant variations affect the electrical lengths *W* and *L* in the same manner and *W/L* remains almost same.

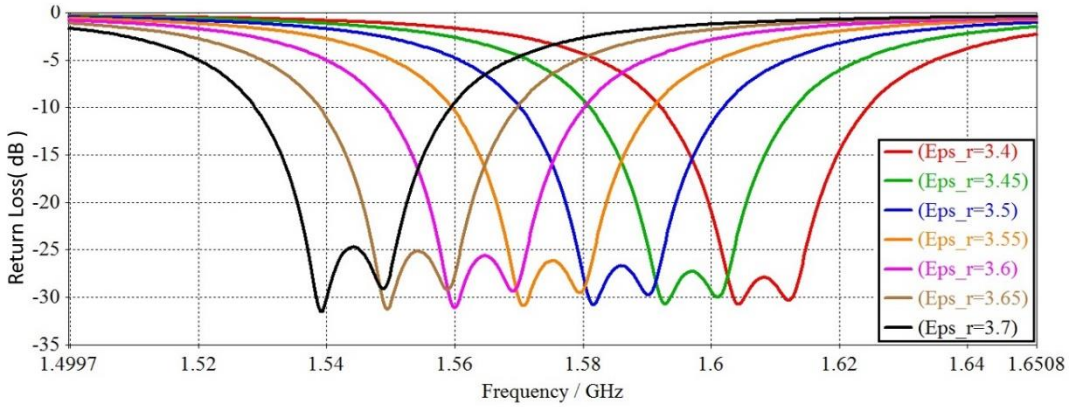

Figure 2-25 Return loss change for various dielectric constants

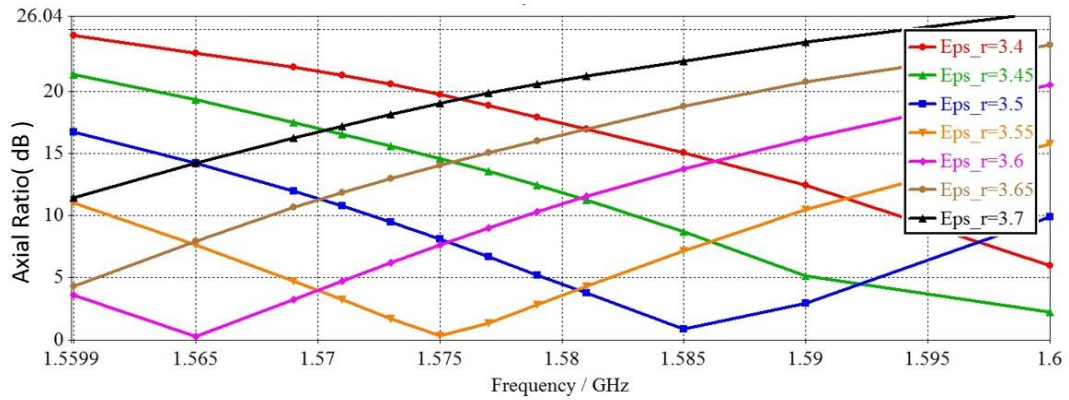

Figure 2-26 Axial ratio change for various dielectric constants

At the beginning of this thesis, FR4 material is chosen in first nearly square patch antenna design. Sensitivity analysis on this antenna is also performed before production. In literature, the dielectric constant of the FR4 material is given as 4.3. Return loss sensitivity analysis for FR4 material wrt. change in dielectric constant is given in Figure 2-27. After manufacturing of the antenna with FR4 material, the center frequency of the antenna was found at 1612 MHz that is nearly 40 MHz higher than the desired GPS L1 band center frequency. When the measured and simulated return loss values are compared, it is concluded that the return loss characteristic of the manufactured antenna is very similar with the simulated one but center frequency is different. According to sensitivity analysis with varying dielectric constant, the return loss measurement of the manufactured antenna was consistent with the antenna that has dielectric constant 4.1. Hence the discrepancy between the measurement and

simulation results of the antenna manufactured on FR4 was most probably due to the dielectric constant variations of this low quality material. To sum up, by performing sensitivity analysis on dielectric constant, the potential reason of manufacturing error in the first antenna design is found.

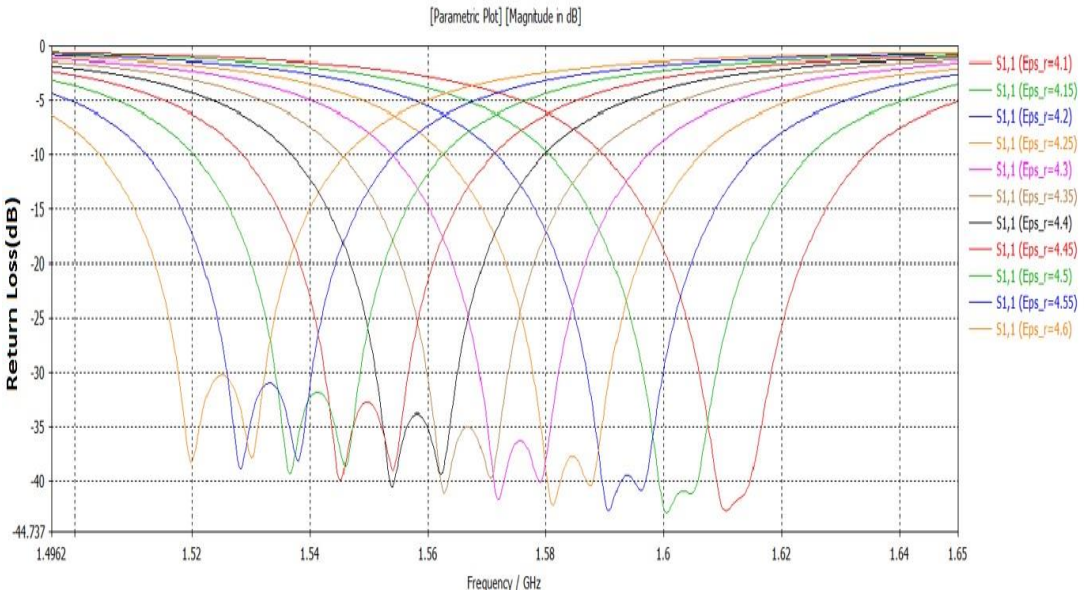

Figure 2-27 Return loss change for dielectric constants of FR4

CHAPTER 3

ACTIVE GPS ANTENNA ARRAY DESIGN

As discussed in the introduction section of this thesis, antenna array provide flexible radiation pattern that maximizes the signal in the desired direction and suppresses the undesired signals. Amplification just after the antenna is necessary in order to decrease overall noise figure. In this chapter; design, manufacturing and measurements of the antenna array are presented in the first section. In the following section, the potential effects of the mutual coupling on the array performance is discussed. At the end of this chapter; design, production and performance of the 4 channel LNA card are introduced.

3.1 Antenna Array Stage

An antenna array is a set of two or more antenna elements. The signals from the antennas are combined or processed in order to achieve improved performance over that of a single antenna. The antenna array can be used to increase overall gain, provide diversity reception, cancel out interference from a particular set of directions, steer the array so that it is most sensitive in a particular direction, determine direction of arrival of the incoming signals and maximize the signal to interference plus noise ratio (SINR) [28]. In this thesis, antenna array is used in order to maximize SINR by steering main lobe toward desired location and null regions toward jammer directions. For antenna arrays, increasing number of elements in array increase the desired performance of the array. Due to the limitations in RF front end and processing units, the number of elements are chosen as 4. Most common array configurations are linear, circular and planar types as shown in Figure 3-1. For 4 element two dimensional arrays, circular and planar configurations result in the same placement of the array elements.

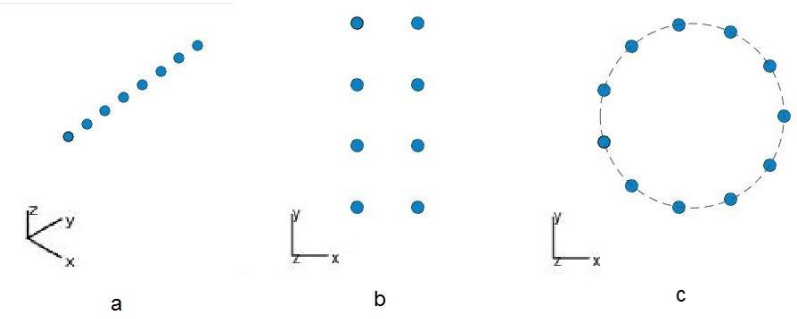

Figure 3-1 Array types a) Linear b) Planar c) Circular

In antenna array theory, if the elements of array are identical and oriented similarly, the total radiation pattern($R(\varphi, \theta)$) can be found with multiplication of radiation pattern of a single element($r(\varphi, \theta)$) and array factor(AF) as shown in equation (3.1).

$$R(\varphi, \theta) = r(\varphi, \theta) * AF \tag{3.1}$$

where φ is the azimuth angle measured from x-axis and θ is the elevation angle measured from z-axis. 4 element circular array is shown in Figure 3-2. 1^{st} element can be accepted as reference element and the AF of this array can be written as shown in equation (3.2) by considering the complex excitation coefficient of i^{th} element to be w_i.

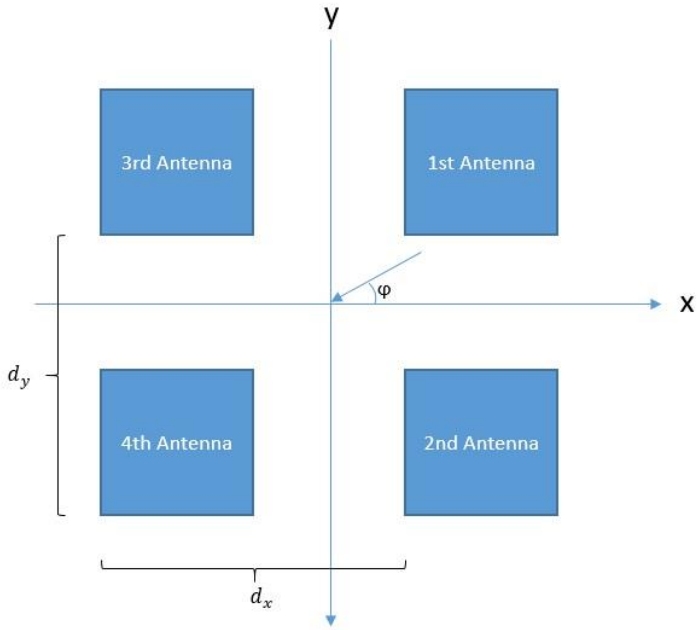

Figure 3-2 Four Element Array and Incoming Angle of Source Representation

$$AF = w_1 + w_2 \times e^{-j2\pi f \frac{d_y \sin(\theta)\sin(\varphi)}{c}} + w_3 \times e^{-j2\pi f \frac{d_x \sin(\theta)\cos(\varphi)}{c}} + w_4 \times e^{-j2\pi f \frac{\sin(\theta)(d_y \sin(\varphi) + d_x \cos(\varphi))}{c}} \quad (3.2)$$

Considering $d_x=d_y=\lambda/2$, AF simplifies to the following form.

$$AF = w_1 + w_2 \times e^{-i\pi \sin(\varphi)\sin(\theta)} + w_3 \times e^{-i\pi \cos(\varphi)\sin(\theta)} + w_4 \times e^{-i\pi(\sin(\varphi)+\cos(\varphi))\sin(\theta)} \quad (3.3)$$

CST MS has two different modules to analyze arrays. In one module it calculates the array factor and multiplies it with the simulated pattern of an isolated element. This approach neglects mutual coupling effects. In the other model, the full-wave analysis of the overall array is performed to include the mutual coupling effects. In this section the former approach is used. Mutual coupling effects will be considered in the next section.

In order to demonstrate the jammer suppression capability of the active array by placing nulls of the array radiation pattern in the direction of the jammers, a scenario with two jammers are investigated. One jammer is placed at $\theta = 79^o$ and $\varphi = 53^o$, and the other one is placed at $\theta = 71^o$ and $\varphi = -101^o$. In order to find the complex weighting coefficients of the array elements, Capon algorithm which will be explained in section 4.1 is used. The azimuth array patterns obtained with these weighting coefficients are shown in Figure 3-3 for $\theta = 79^o$ and in Figure 3-4 for $\theta = 71^o$. As it can be observed from these figures, nulls of the radiation pattern are successfully placed at the direction of jammers.

4 element array is analyzed in CST MS. The CP antenna which is designed for RO4003 material with 1.524 mm is used as the array element. It should be noted that after 4 element array is manufactured and measured, it is realized that AR bandwidth shifts out of L1 band due to mutual coupling effects in the array environment. Hence the element design is changed to the one with thicker substrate to obtain wider bandwidth so that the desired CP operation is achieved in spite of the frequency shift in the array environment.

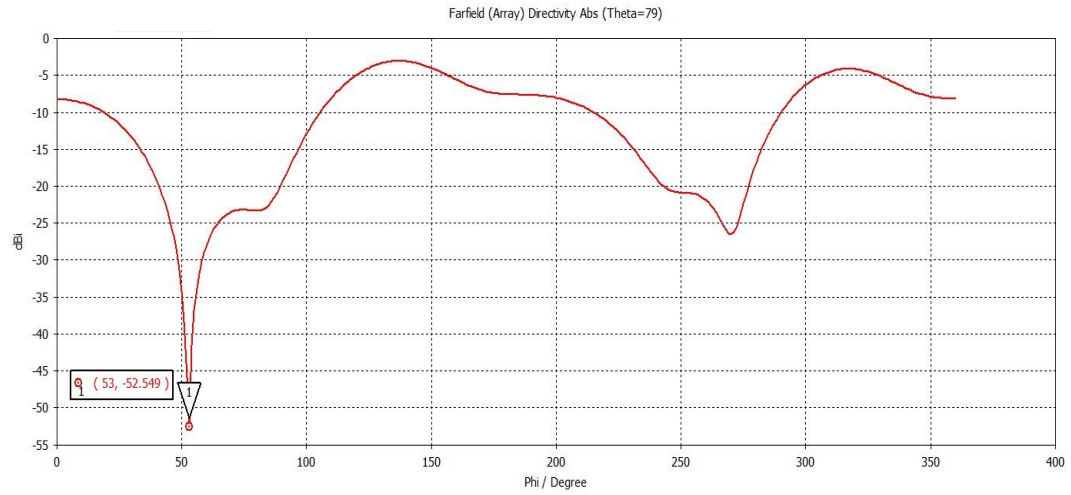

Figure 3-3 Azimuth Pattern at $\theta = 79^o$

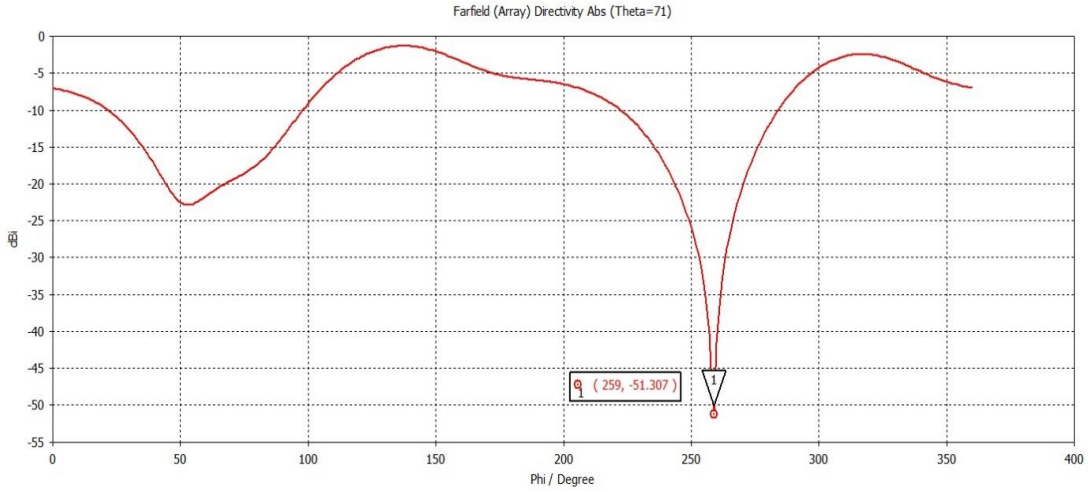

Figure 3-4 Azimuth pattern $\theta = 71^o$

However this design was concluded quite later, so the studies on the array is continued with the element on thinner substrate. Circular ground plane and dielectric substrate is used for the array and the radius of the ground plane is 135 mm. The antenna structure of simulated array is shown in Figure 3-5.

The comparison of return losses for each element is shared in Figure 3-6. According to return loss simulations, all antennas in the array seems identical in terms of radiation properties. However, when these simulation results are compared with the simulation results of the isolated element, shift in center frequency is observed.

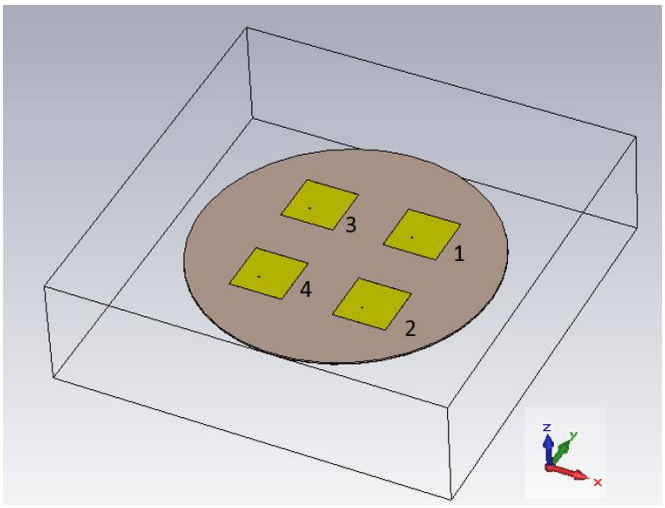

Figure 3-5 Four Element array model in CST MS

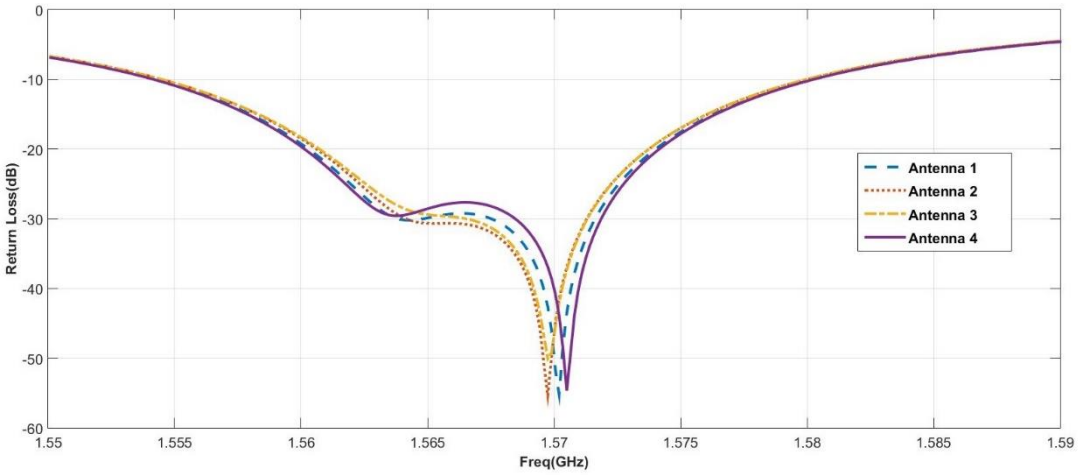

Figure 3-6 Return loss comparison of array elements in CST

In order to get better understanding of array performance, axial ratio simulations can be investigated as shown in Figure 3-7. It can be observed that AR center frequency of AR bandwidths are shifted below the center frequency of the isolated element when antenna is put into array. In addition to this, two different characteristics are observed between elements. The cross elements show very similar polarization properties. If we look at AR bandwidths, 2nd and 3rd antennas show similar characteristics as the isolated element. However, the center frequency for the 1st and 4th antenna in the array is almost 4 MHz smaller than 2nd and 3rd antenna and the AR bandwidth is also smaller than these antennas. Before detailed investigation on reasons of these differences, it has

been decided to manufacture the antenna array and compare the simulation and measurement results.

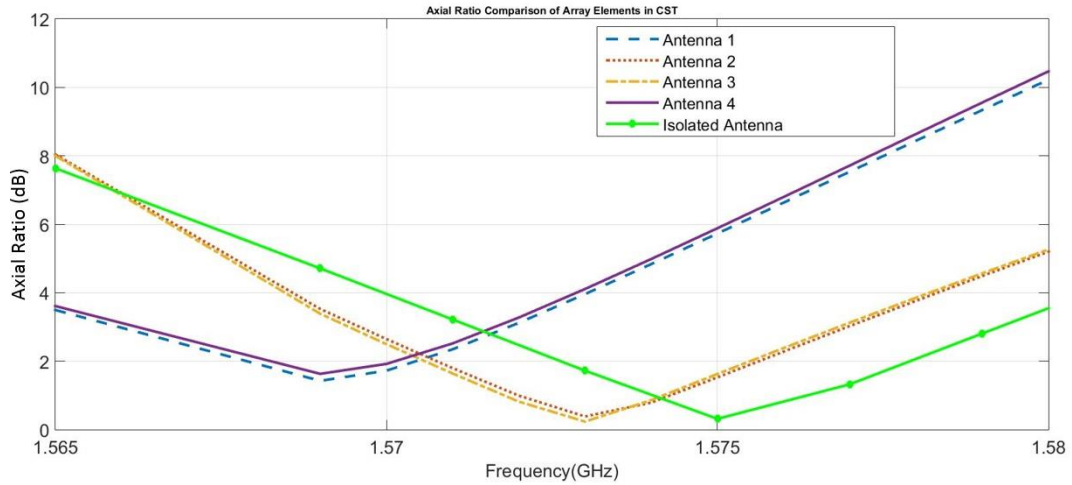

Figure 3-7 Axial ratio comparison of array elements in CST

4 element array manufactured with LPKF machine as shown in Figure 3-8. The measured return loss results of all elements and the isolated element is given in Figure 3-9. In this figure, return loss properties for all elements seem identical but a frequency shift compared to isolated element is observed similar to the observations in simulations.

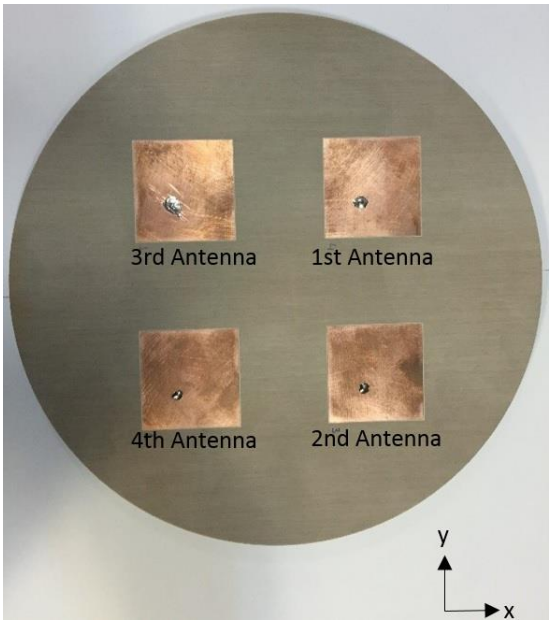

Figure 3-8 Produced 4 element antenna array

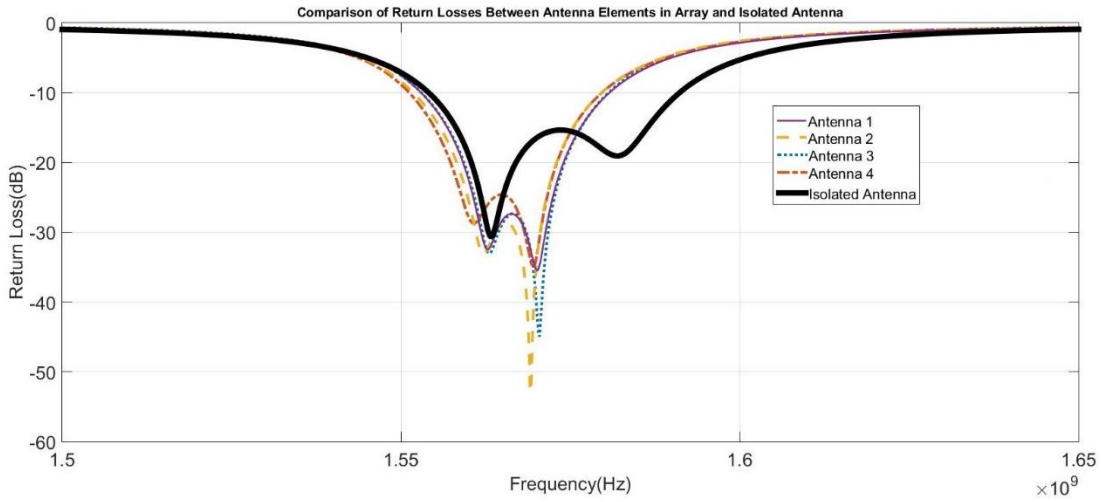

Figure 3-9 Return loss measurements of array elements and isolated element

In AR measurements, a transmit antenna is kept fixed and the antenna that is wanted to be measured is rotated around its axis. AR measurement process is performed for all frequencies that is defined by system user. AR measurements are performed in anechoic chamber that is placed in Ayaslı Research Center and the picture from the AR measurements is shown in Figure 3-10. AR measurements of all elements are given in Figure 3-11 with AR results of isolated element. Similar to the observations in simulation results, the AR bandwidth shifts more for Antenna 1 and Antenna 4.

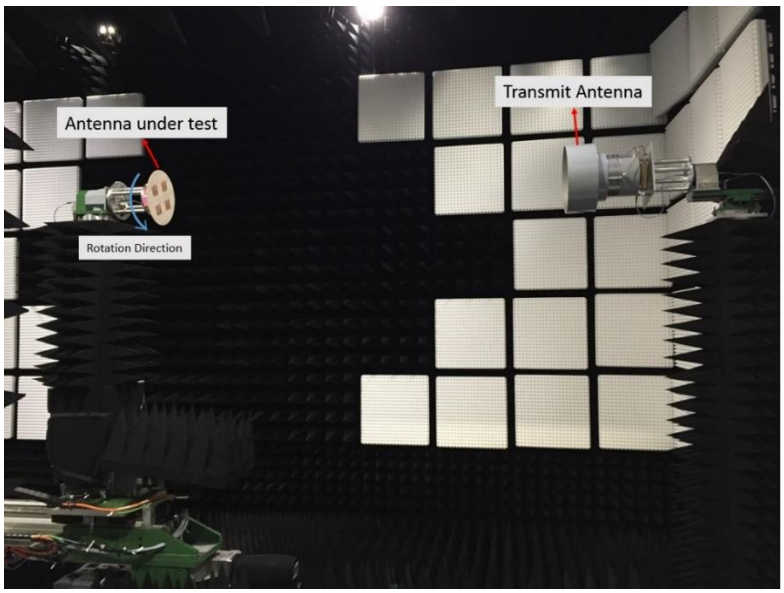

Figure 3-10 Anechoic room-Axial ratio measurements of antenna array

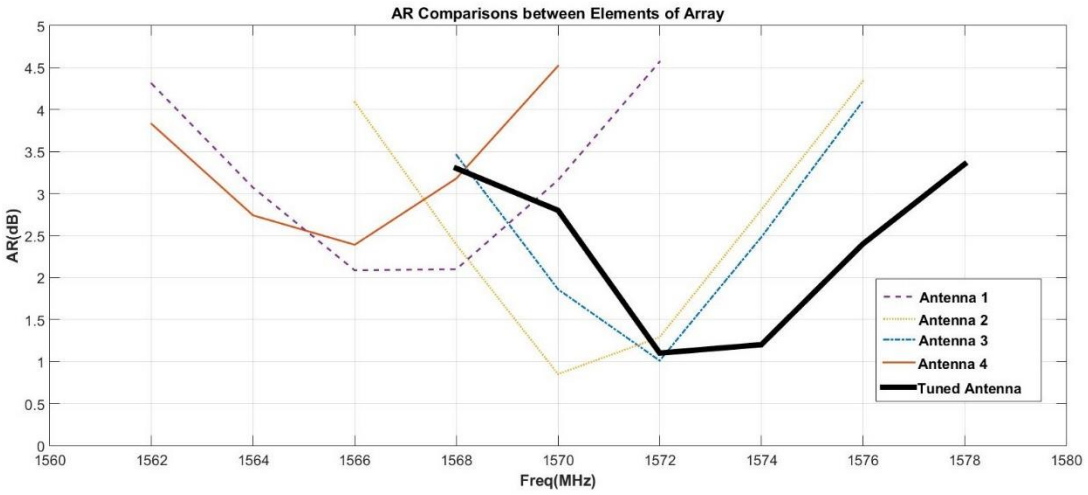

Figure 3-11 AR comparison of array elements and isolated antenna

Since the mutual coupling between the array elements results in such a degradation in the array performance, it will be studied in more detail in next section.

3.2 Effect of Mutual Coupling on Array Performance

Mutual coupling can be defined as the electromagnetic interaction between different objects or between different parts of a single object. The effects of the mutual coupling on the array performance depend upon the antenna type, relative positioning of the elements in the array, feed structure and scan volume of the array [19]. Mutual coupling is an inevitable effect for antenna arrays and it can change the array radiation pattern, array manifold and matching characteristics of the antenna elements. The return loss and polarization properties of the antenna are related with the matching properties, unexpected differences between individual antenna and antenna in array become possible as observed in Figure 3-10 and Figure 3-11. In order to investigate whether the shape and size of the ground plane affect the amount of mutual coupling, a 4 element circular array with nearly square ground shape as shown in Figure 3-12 is analyzed in CST MS. Since mutual coupling is observed to be more effective on polarization characteristics, only AR comparison of the elements in new array configuration is studied. In Figure 3-13, the AR results for the elements of the new antenna array configuration and isolated antenna element are given. When AR results, are investigated, it can be concluded that mutual coupling doesn't affect the center frequency of the antennas considerably. Comparing with the results given in Figure 3-7 for circular ground plane, this new array configuration seems better in order to

avoid mutual coupling effects as much as possible. The reason of this might be related to the scattering and diffraction that each edge of each antenna experience. Recall from transmission line theory that radiating edges of a microstrip antenna can be modeled by an equivalent slot. In a CP antenna all 4 edges are radiating edges. As it can be observed from Figure 3-12, for antenna 3, edges 1 and 2 interact with the adjacent antenna elements and edges 3 and 4 interact with the edges of the ground plane. Since all the radiating slots are affected CP operation is preserved. However for circular and larger ground plane, while field distributions at edges 1 and 2 will be disturbed by other elements, field distributions at edges 3 and 4 will not be affected. Hence this unbalance may cause degradation in CP operation.

On the other hand, like in the case of circular ground plane, the AR performance of the cross elements (2 and 3, 1 and 4) are similar. The answer of the question why mutual coupling doesn't affect all elements symmetrically may be the feed locations of the antennas.

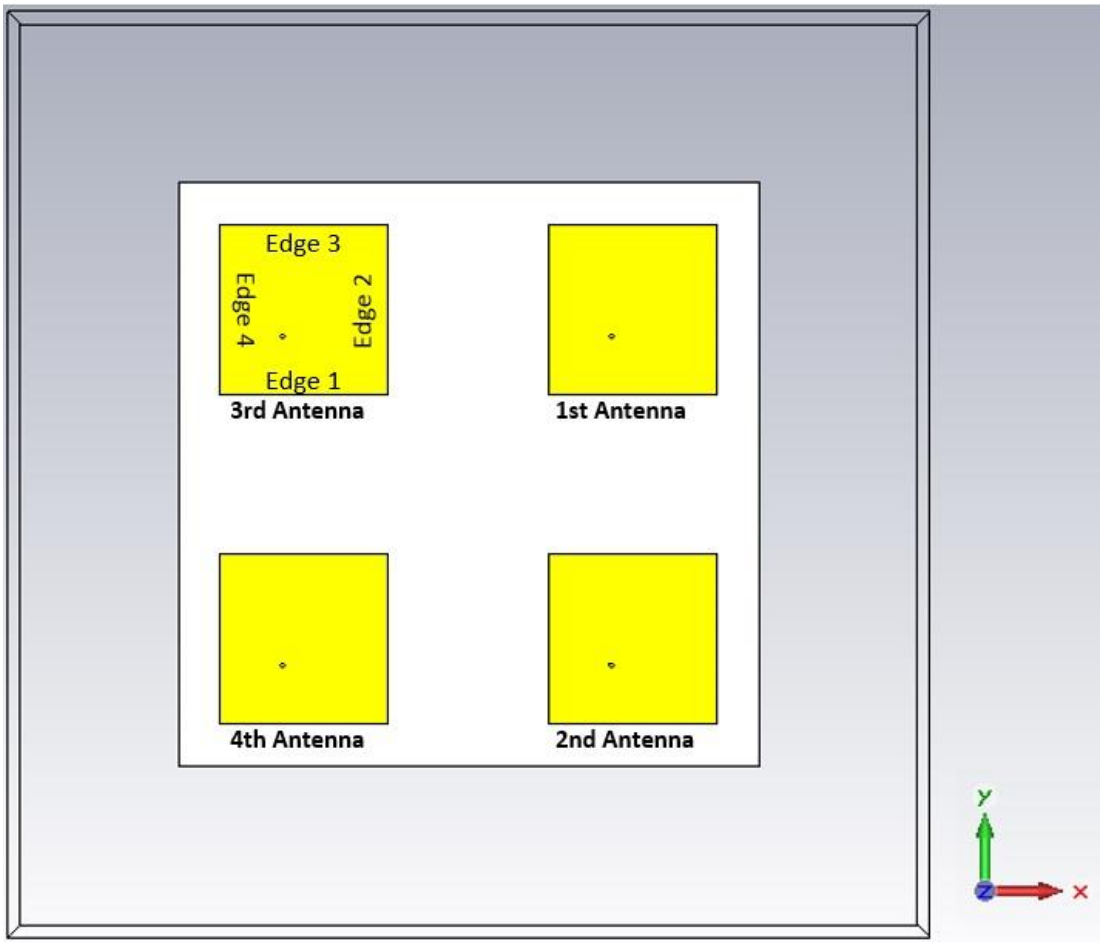

Figure 3-12 4 element planar array with new ground shaping

Eventhough the mutual coupling effects can be reduced slightly by changing the size and shape of the ground plane, total elimination of those effects is not possible. Moreover, tuning of the antenna elements (either experimentally or through simulations) within the array environment is not practical since a change in one antenna affects the performance of the other, the best design approach would be to design antennas with wider bandwidths that could tolerate the effects of mutual coupling.

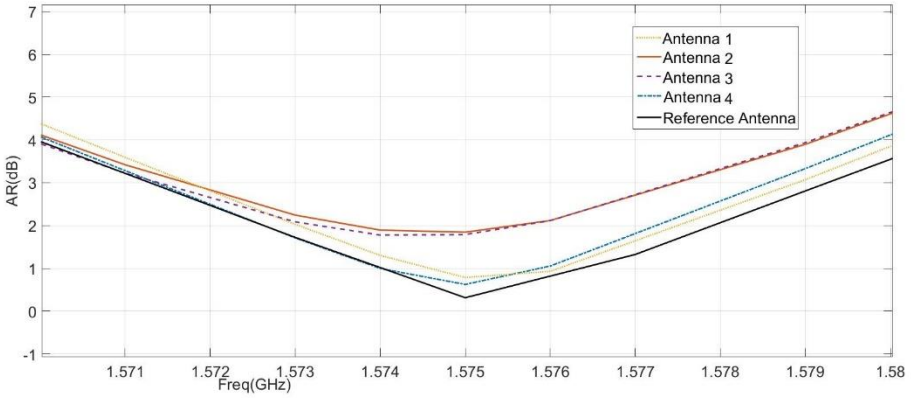

Figure 3-13 AR Comparison between Array Elements and Reference Element

3.3 4 Channel LNA Stage

In RF front end design, overall noise figure of the system is a very important parameter. As in any other system, additive noise and degradation of SNR in GPS receiver is unwanted. Considering f_n as the noise figure of the n^{th} element in cascade system and g_n as the gain of the n^{th} element in a cascaded system, the overall noise figure f_s can be expressed as,

$$f_s = f_1 + \frac{f_2 - 1}{g_1} + \frac{f_3 - 1}{g_1 g_2} + \cdots + \frac{f_n - 1}{g_1 g_2 g_3 \cdots g_{n-1}} \qquad (3.4)$$

It can be concluded from this equation that first element in the cascaded system dominates the overall noise figure. According to this, passive components prior to the first amplifier will severely degrade the noise figure. For GPS, the cable between antenna and RF front end is very long except for hand held device applications. If there is no amplifier prior to this long cable, there will be serious decrease in SNR. However,

if an amplifier is incorporated within the antenna prior to long cable, noise figure performance is increased. This implementation is applied in many systems and known as active antenna [2]. Hence it is decided to design active antenna array for this GPS application. In this work, since the data from 4 antennas in array are processed separately, 4 channel LNA card is needed. For LNA card design, wideband LNA integrated circuit is chosen in order to use it in multi frequency GNSS receiver applications in future. The chosen LNA IC was PMA4-33GLN+ from Mini Circuits. This LNA works between 0.7 GHz and 3 GHz with varying amplification performance according to working frequency. During design process, Altium Designer program is used. In schematic preparation, the reference design given in datasheet of the product is utilized [29]. For schematic of LNA card, one channel is prepared as shown in Figure 3-14. In PCB preparation, same schematic is used for all channels in the card. After production of the PCB and soldering of the components, the 4 channel LNA card was ready for performance tests. The top and bottom sides of LNA card is shown in Figure 3-15. The LNA card is designed to be located below antenna array. In order to make compact design, the SMA connectors for the RF inputs of the LNA card are placed in top side of the card while SMA connectors for the outputs of the LNA are placed in bottom side of the card. The pictures that show cabling between the antenna array and 4 channel LNA card are shown in Figure 3-16. The amplification performance of the LNA card can be understood from the comparison of measured values and values that are reported in datasheet of LNA IC as listed in Table 3-1. According to gain comparison result, amplification performance is smaller than the values given in datasheet. It should be noted that the reported gain values are the maximum available gain of the IC only. The difference may be due to the loss introduced by the total PCB design with all other components.

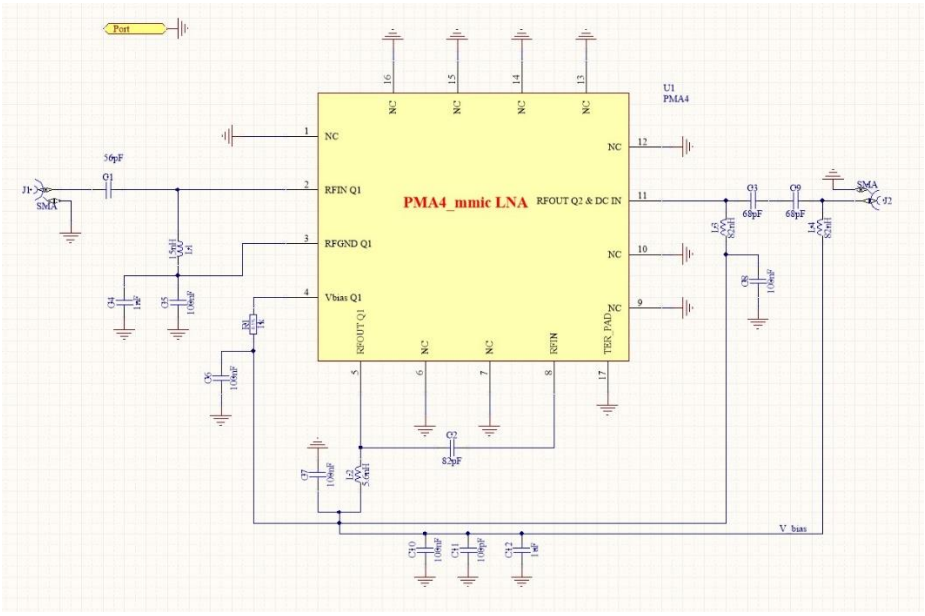

Figure 3-14 Schematic of one channel in LNA card

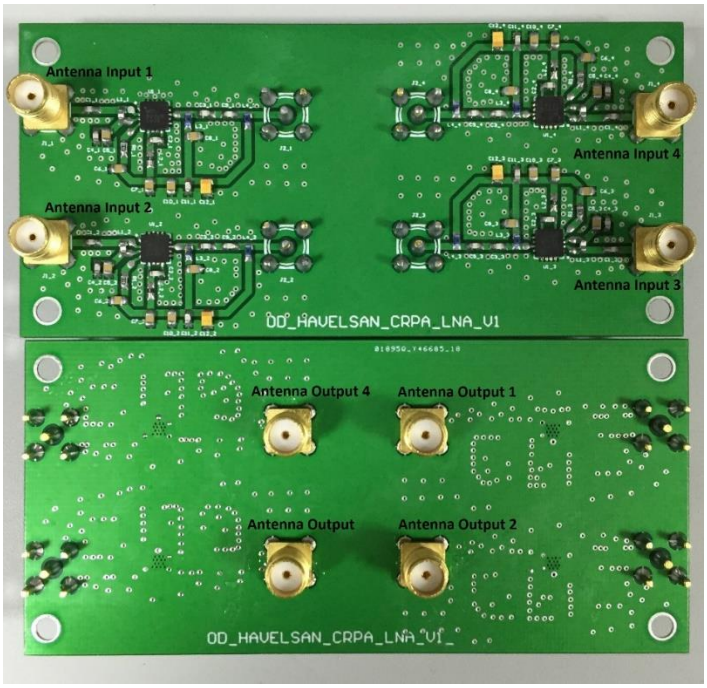

Figure 3-15 Top and bottom sides of 4 channel LNA card

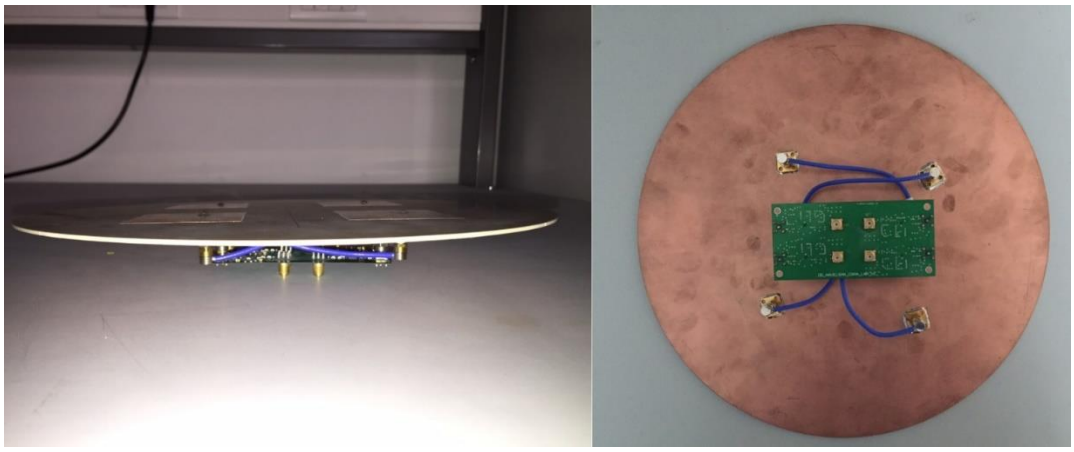

Figure 3-16 Active antenna array

Table 3-1 LNA card gain comparison table

	0.7 GHz	0.9 GHz	1.5 GHz	2 GHz	3 GHz
Measured Gain(dB)	38.94	36.14	28	23	17
Given Gain(dB)	41.3	38.9	31.8	26.9	18

CHAPTER 4

BEAMFORMING APPROACHES FOR JAMMING SUPPRESSION

Array signal processing is a technique to get better performance than single antenna by processing the data coming from each element in the antenna array. Beamforming with many alternative methods is counted in array signal processing class and can be classified as spatial filtering. Beamforming methods can be classified as conventional and adaptive beamforming. Conventional techniques use fixed set of weights and fixed pattern. However, adaptive techniques use the received data to specify weighting coefficients of each antenna. Adaptive techniques can also be separated as blind and non-blind beamforming. For non-blind beamforming algorithms, there is reference information about received data or incoming direction of the target signal. If there is no information about the received data, blind beamforming techniques are necessary. Since obtaining reference signal for GPS application is very difficult, reference signal based beamforming methods are not applicable for GPS antijamming purposes.

In this thesis, two adaptive beamforming algorithms are implemented. These algorithms are Capon beamforming approach and null steering. Capon beamforming approach needs only the incoming direction of the target signal and classified as non-blind approach. In GPS antijamming application, the target signal is the signal coming from any GPS satellite. There is no necessity to know information about the incoming direction of the jammer signals. Because the position of the satellites in the sky is known with almanac data, this information can be used as an input to Capon beamforming algorithm. For null steering algorithm, there is need for both the direction of jammer and target signals. Target signal is again GPS satellites and positions are known at each time of the day. However jammer directions aren’t known.

Therefore, the direction of jammers need to be estimated by employing direction of arrival (DOA) algorithms.

4.1 Capon Beamforming Approach

Capon beamforming method provide adaptive choice of complex weighting coefficients that maximize SINR and provide distortionless response in the direction of target signal [30]. Capon algorithm only need the direction of the target signals as mentioned at the beginning of this chapter. Therefore, this algorithm can be used in GPS applications with jamming suppression purpose. With Capon beamforming application, the main beam of the antenna looks toward GPS satellite while the null regions are directed to jammer sources.

The received data of an *M* element antenna array can be expressed with *X* vector of length M that contain target signal *S*, interference signal *I* and overall noise *N* as shown in equation (4.1).

$$X = S + I + N \tag{4.1}$$

The *MxM* cross covariance matrices of the received data and interference signal are expressed as R_x and R_{IN} that are given with equation (4.2) and equation (4.3), respectively for *K* number of snapshots.

$$R_x = \frac{1}{K}\sum_{k=1}^{K} XX^H \tag{4.2}$$

$$R_{IN} = \frac{1}{K}\sum_{k=1}^{K} (I+N)(I+N)^H \tag{4.3}$$

The purpose of the Capon beamforming approach is to maximize SINR that is expressed with equation (4.4) while maintaining the distortionless response toward target signal source. In other words, Capon beamforming method is looking for the solution of the following linearly constrained quadratic problem where *a* is the steering vector of the target signal and given in equation (4.5) for the four element antenna array that is shown in Figure 3-2.

$$\min_{w} w^H R_{IN} w \;\; subject\ to \;\; w^H a = 1 \tag{4.4}$$

$$AF = [1; e^{-jk\frac{\lambda}{2}\sin(\theta)\sin(\varphi)}; e^{-jk\frac{\lambda}{2}\sin(\theta)\cos(\varphi)}; e^{-jk\frac{\lambda}{2}\sin\theta(\sin\varphi+\cos\varphi)}] \quad (4.5)$$

The solution of the problem in equation (4.4) with Lagrange Multiplier method gives optimum weighting vector w_{opt} that put nulls in jammer directions and maximizes the target signal and w_{opt} can be found with equation (4.6) where a is the steering vector.

$$w_{opt} = \frac{R_{IN}^{-1}a}{a^H R_{IN}^{-1}a} \quad (4.6)$$

Because interference signal is not known under jamming threat, R_{IN} cannot be calculated. However, R_{IN} can be approximated as R_x under jamming threat. Therefore w_{opt} can be found with equation (4.7).

$$w_{opt} = \frac{R_x^{-1}a}{a^H R_x^{-1}a} \quad (4.7)$$

After desired complex weighting vector is found, the output signal y that includes GPS signal purified from jammer can be calculated with the following formula.

$$Y = w_{opt}^H X \quad (4.8)$$

Performance test of Capon beamforming approach is first performed in MATLAB. A modulated signal is created in MATLAB and transmit it with GPS L1 carrier frequency. A circular array with omnidirectional elements is designed in MATLAB. White gaussian noise is used as a jammer source. Capon beamforming algorithm is applied to the received data by antenna array in MATLAB and the performance of Capon Beamforming approach is observed. In these tests, the number of snapshots is taken as 500 because performance is observed acceptable with this value.

4.1.1 Example Scenario-One Jammer and One Target Signal

For this scenario, the jammer suppression test is performed with varying jammer power level. In addition, jammers and target are located at different places and tests are repeated. In all of these test, algorithm has showed similar performance. In one of the tests, the target is created with specific modulation and applied from 54^o azimuth and 71^o elevation angle. Note that, elevation angle is measured from ground surface in this chapter. In this test, one jammer is used and applied from -29^o azimuth and 13^o elevation angle. The direction of the target signal is an input to the algorithm. The modulated transmitted signal that is received from one of the elements in array is shown in Figure 4-1 (a). After jammer is applied, the received signal from one of the elements in the array is shown in Figure 4-1 (b). As it can be seen from the figure, the

modulated signal is lost under jammer signal and there is no information coming from target source.

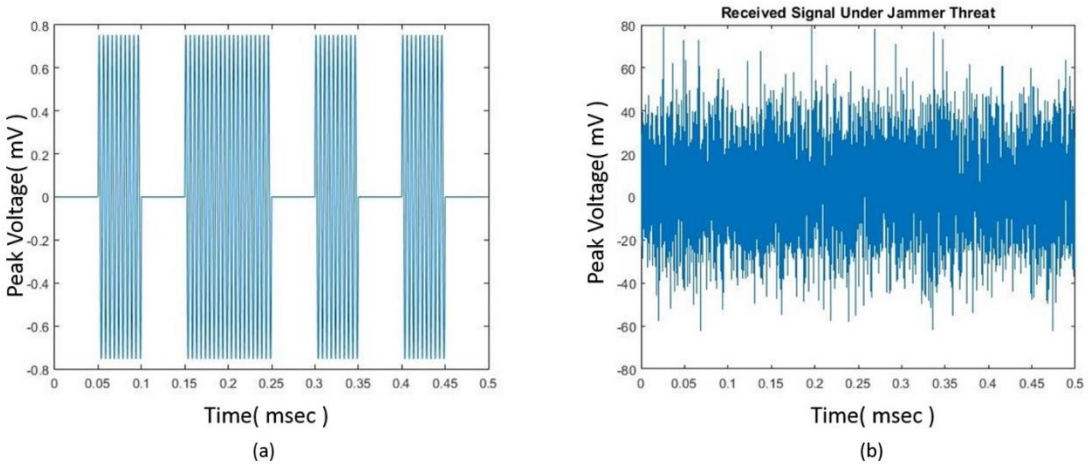

Figure 4-1 a) Modulated target signal b) Received signal under jammer threat

After application of the Capon beamfoming approach to received data from 4 element antenna array, jammer is suppressed and target signal is extracted with small noise on it as shown in Figure 4-2.

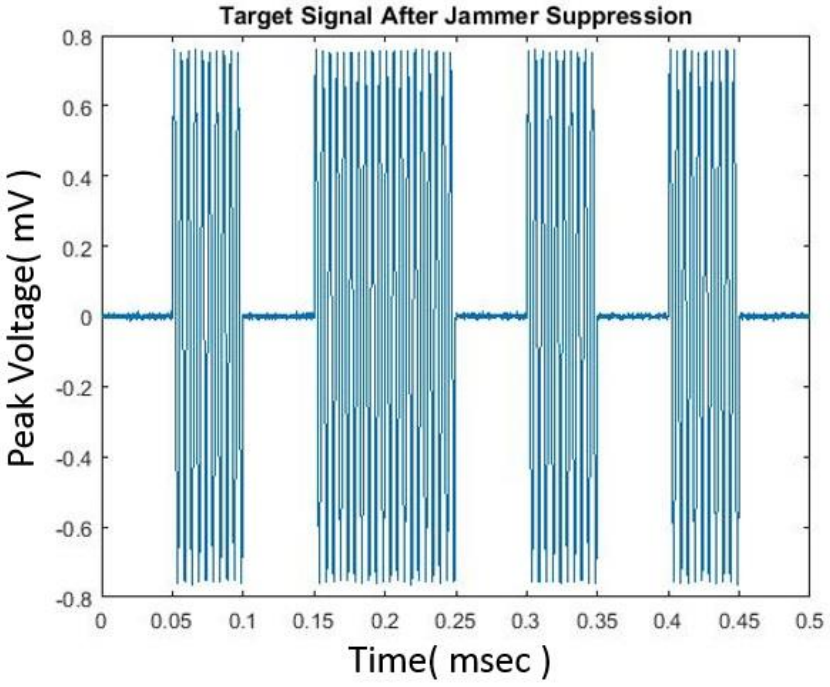

Figure 4-2 Target signal after jammer suppression

The weighting coefficients that are obtained with application of Capon beamforming algorithm give radiation patterns in the plane of target sources ($\theta = 71^o$) and in the plane of jammer ($\theta = 13^o$) are shown in Figure 4-3 (a) and (b), respectively. The purpose of Capon beamforming algorithm is to put null in jammer region and steer main lobe to target signal. Results given in Figure 4-3 (a) and (b) verify the performance of the algorithm.

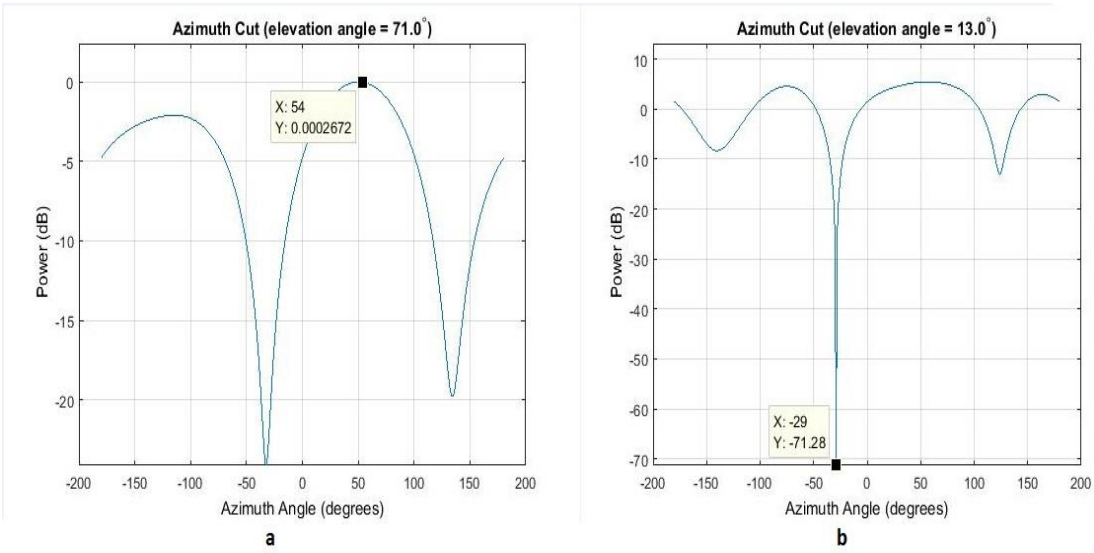

Figure 4-3 Radiation Pattern a) In the plane of target b) In the plane of jammer

In this scenario, jammer to signal ratio was set as 30 dB. Jammer suppression level was 75 dB. Therefore, the target signal is obtained with almost zero distortion.

4.1.2 Example Scenario-Two Jammer and One Target Signal

For this scenario, two jammer sources and one target sources are applied from different directions. A lot of simulations are performed and the jammer suppression performances were very similar. In one of the experiments, one modulated signal is transmitted with GPS L1 carrier frequency from -38º azimuth and 53º elevation angle. One of the jammer sources is located in -127º azimuth and 18º elevation angle. The other jammer source is applied from 63º azimuth and 29º elevation angle. The target modulated signal is same with signal used in section 4.1.1. Under two jammer sources threat, the received signal from one of the antennas is shown in Figure 4-4. Again the modulated signal is lost under jammer threat.

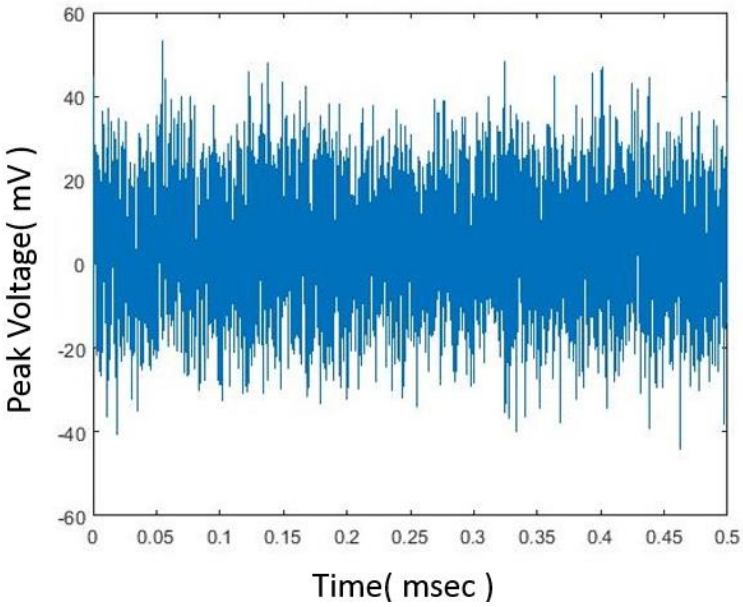

Figure 4-4 Received signal when two jammers are active

After application of the Capon beamforming algorithm to data received by 4 element antenna array, the jammers are suppressed and modulated target signal is extracted as shown in Figure 4-5 (a). The radiation pattern in the plane of target signal is given in Figure 4-5 (b). In this figure, it is shown that the distortionless response is provided in target direction. The radiation patterns in the planes of the jammer sources are given in Figure 4-6 (a) and (b). As it can be seen from these figures, the weighting coefficient that is obtained by application of Capon beamforming algorithm put null regions where jammer sources are exactly coming from.

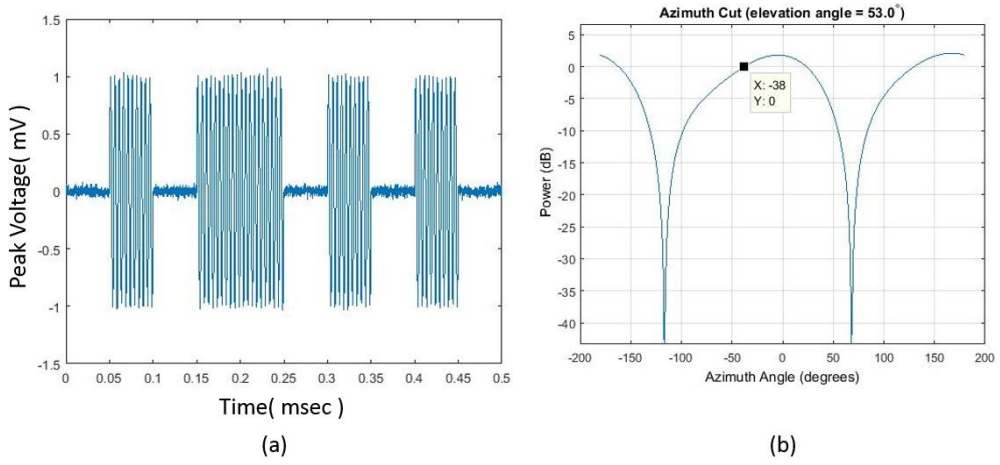

Figure 4-5 a) Target signal after jammer suppression b) Radiation pattern in the plane of target signal

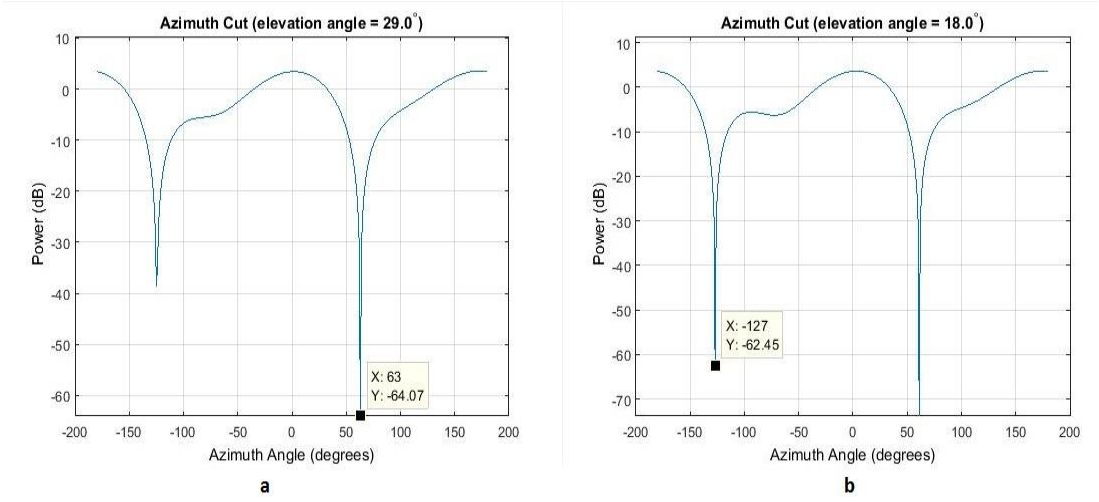

Figure 4-6 Radiation Pattern a) In the plane of 1st interference b) In the plane of 2nd interference

In this scenario, the power levels of jammer sources and target source were same with the scenario 1. However suppression rate of jammers was nearly 65 dB. Therefore the extracted signal from two jammer sources has more noise on it. From this suppression level, it can be concluded that the jammer suppression performance of the Capon beamforming approach decreases with the increase in number of jammer sources. With 4 element antenna array, there is possibility to suppress 3 jammer sources. With 3 jammer sources, the suppression performance of the Capon beamforming approach is observed to be more dependent on the direction of the jammer sources and to be not so stable.

In conclusion, according to MATLAB simulation results, the jammer suppression performance of the Capon beamforming approach is satisfying. Hence this algorithm is decided to be used in real time experiments.

4.2 DOA Estimation of Jammer and Null Steering

Null steering is the second approach to suppress jammer sources to protect GPS receivers. Null steering is one of the oldest beamforming algorithms. It was a different kind of multiple sidelobe cancellers developed by P.Howells[31] and soon after by S.Applebaum[32]. Null steering needs both direction of the target signal and jammer signals. In GPS antijamming application, target signal is coming from again GPS

satellite and the positions of satellites are known with almanac data. Because direction of jammers aren't known, application of DOA algorithm is necessary to find jammer directions. In this thesis, MUSIC algorithm is used to estimate coming directions of jammer sources. MUSIC is an abbreviation of multiple signal classification that is one of the high resolution subspace based DOA algorithm and extracts the direction of sources [33].

4.2.1 DOA estimation of Jammer Sources with MUSIC Algorithm

The basic idea of the DOA estimation with MUSIC algorithm is separating the signal and noise by using orthogonality property of their spaces. This can be achieved with eigendecomposition of the correlation matrix of the received signal. Because noise signals in each channel are uncorrelated and jammer signals are correlated, correlation matrix includes information about the number of jammer signal sources and strength. Considering M as an antenna element number in array and K number of received snapshots, the covariance matrix R_x can be created with equation (4.2). After eigendecomposition of the correlation matrix, eigenvalues ($\lambda_0,\lambda_1,\ldots,\lambda_{M-1}$) and eigenvectors($q_0,q_1,\ldots,q_{M-1}$) are found such that λ_0 is the largest eigenvalue and λ_{M-1} is the smallest eigenvalue. While using MUSIC algorithm, the number of jammer sources should be known. Since the eigenvalues of the correlation matrix depend on the power levels of signals sources, the number of jammer sources can be extracted from the relations between eigenvalues. In simulations with MATLAB, the number of jammer source is considered to be the number of eigenvalues that are significantly larger than the others. Considering the number of jammer sources are D, the eigenvalues from λ_D to λ_{M-1} are extracted and the corresponding eigenvectors to these eigenvalues create the noise subspace as given with equation (4.9).

$$V_n = [q_d \; q_{d+1} \ldots \ldots \ldots q_{M-1}] \tag{4.9}$$

Because the jammer signal and noise subspace are orthogonal, the following equation is valid considering θ and φ as an incoming angle and a as a steering vector of the jammer signal.

$$a^H(\varphi,\theta)V_nV_n^H a(\varphi,\theta) = 0 \tag{4.10}$$

Then the DOAs of the jammer signals can be found by looking the peaks in the MUSIC spatial spectrum that is given by equation (4.11).

$$P_{music}(\varphi,\theta) = \frac{1}{a^H(\varphi,\theta)V_nV_n^Ha(\varphi,\theta)} \quad (4.11)$$

DOA estimation accuracy of the MUSIC algorithm can depend on the number of taken snapshots and number of elements in the array. If the environment is stable and all systems are constant, increased number of snapshots give sharper spectrum. In addition, increased number of elements in array also give sharper spectrum and increase the DOA accuracy. In [34], there is simulation work about the previously mentioned effects in MUSIC spectrum. These effects are tried and verified in MATLAB. In the following subsections, some experimental results of DOA estimation performance is presented

4.2.1.1 Example Scenario-One Jammer Source

In the first experiment the same scenario that is used for Capon algorithm is repeated. Jammer is placed in -29^o azimuth and 13^o elevation angle. Target signal is again located in 54^o elevation and 71^o azimuth. After eigendecomposition of the correlation matrix, eigenvalues are found as 1.238e5, 48.13, 0.25 and 0.24. Since biggest eigenvalue is not closed to following biggest eigenvalue, it can be said that there is one jammer source. After application of MUSIC algorithm, the MUSIC spectrum in 3D and 2D is found as shown in Figure 4-7 (a) and (b), respectively. The MUSIC spectrum index shown in the figures is between 1 and 360 that corresponds to azimuth angle between -180^o and 180^o. In addition, the real elevation angle of the jammer is one defeat of the shown value due to indexing of the matrix. Therefore, sharp peak that is found in MUSIC spectrum is located in 13^o (14-1) elevation angle and -29^o (152-181) azimuth angle which is consistent with the given scenario.

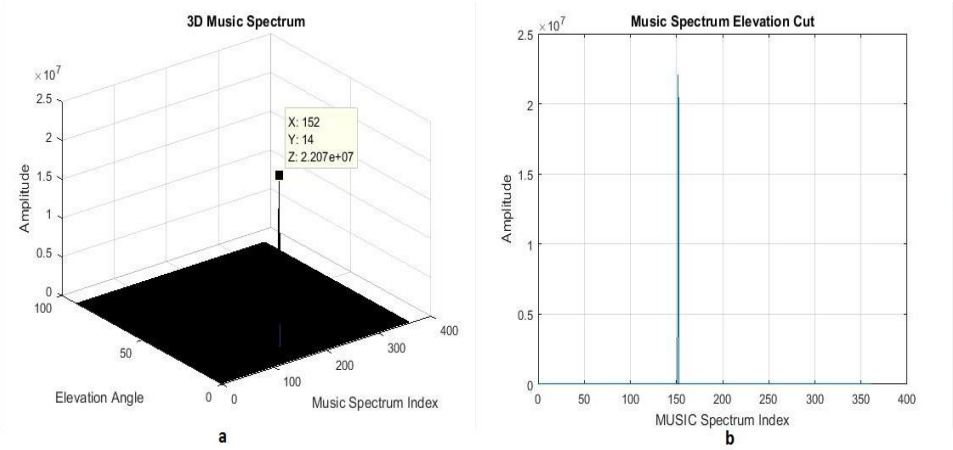

Figure 4-7 MUSIC spectrum under one jammer source a) 3D b) 2D

4.2.1.2 Example Scenario-Two Jammer Sources

In another experiment, two jammer sources are used as a threat to target signal. The location of jammer sources were same with the scenario given in section 4.1.2. After eigendecomposition of the correlation matrix, the eigenvalues are found as 1.319e5, 1.2161e5, 47.26 and 0.25. The algorithm detected existence of two jammer sources from eigenvalues and applied MUSIC algorithm to find locations of them. 3D Music spectrum is given in Figure 4-8.

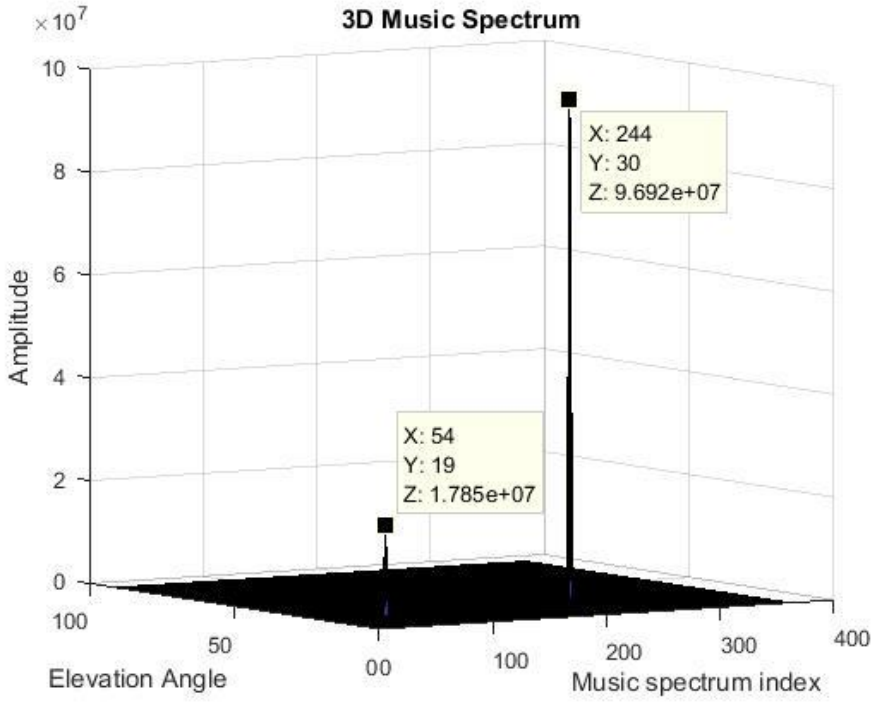

Figure 4-8 3D music spectrum under two jammer sources

With explanation about the index of MUSIC spectrum, one of the jammers is located in 63^{o} (244-181) azimuth and 29^{o} (30-1) elevation angle. The other jammer is located in -127^{o} (54-181) azimuth and 18^{o} (19-1) elevation angle. When these results are compared with the actual locations of jammers, it can be concluded that the DOA estimation performance of the MUSIC algorithm is perfect.

In tests with 3 sources, MUSIC spectrum give instable results in terms of accuracy. If the DOA performance is not good, the jammer suppression performance of the null steering algorithm is directly affected. When number of jammer is less than 3, MUSIC algorithm generally gives accurate DOA results.

4.2.2 Null Steering with Known Target and Jammer Signal Directions

In application of the null steering algorithm, it is aimed to direct the main lobe toward target direction and null regions toward jammer source directions. The position of the satellites are known with almanac data. After finding the jammer direction with the MUSIC algorithm, null steering algorithm can be applied with jammer suppression purpose. Considering *N* as the number of elements in the array and *L* as the number of jammer sources, *v(k)* represents the steering vector of the target and $v(k_i)$ (i=1,2,…,L) represents the steering vector of the jammers. Using steering vector of the target and jammer sources, *A* matrix can be formed by using the following relation,

$$A = [v(k)^H; v(k_1)^H; \dots; v(k_L)^H] \tag{4.12}$$

In usage of null steering algorithm, the complex weighting coefficient w can be calculated solving the following equation,

$$Aw = s \tag{4.13}$$

where *s* is the result vector and expressed with the following relation,

$$s = [1; 0; \dots; 0] \tag{4.14}$$

When the number of jammer sources are less than one defeat of the number of antennas in array, the weighting coefficient vector can be solved with minimum norm technique and it can be expressed by equation (4.15).

$$w = A^H(AA^H)^{-1}S \tag{4.15}$$

If the number of jammers is equal to one less of number of the antennas in array, weighting coefficient vector can be obtained with simple matrix inversion technique as given in equation (4.16).

$$w = A^{-1}s \tag{4.16}$$

4.2.2.1 Example Scenario-One Jammer and One Target Signal

This scenario is exactly same with scenario in section 4.1.1. The target signal is same modulated signal and jammer is again white Gaussian noise. The direction of jammer source is found with MUSIC algorithm application and null steering is performed. The radiation pattern in the plane of target signal and received signal after toward target signal and extracted signal after jammer suppression are shown in Figure 4-9. The radiation pattern in the plane of jammer source is given in Figure 4-10.

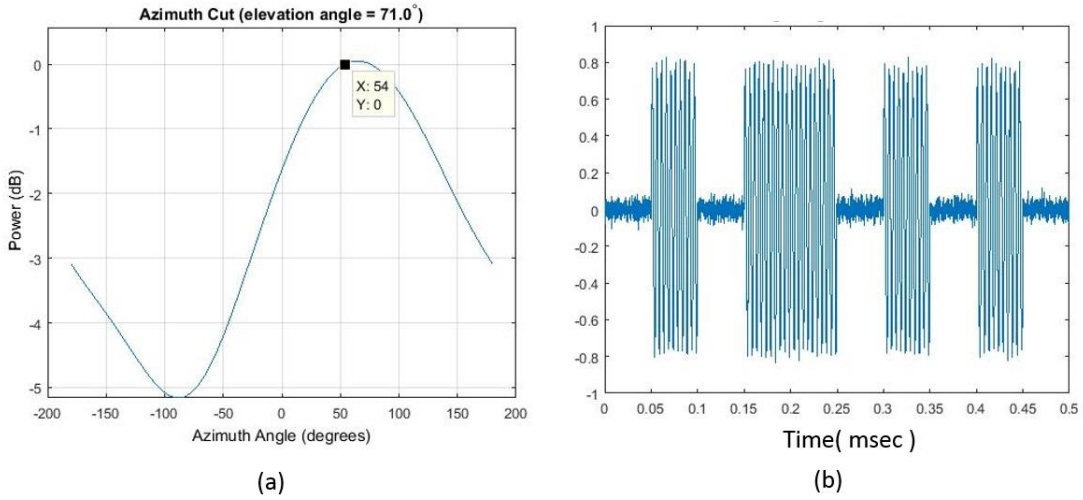

Figure 4-9 a) Radiation pattern in the plane of target signal b) Received signal after jammer suppression

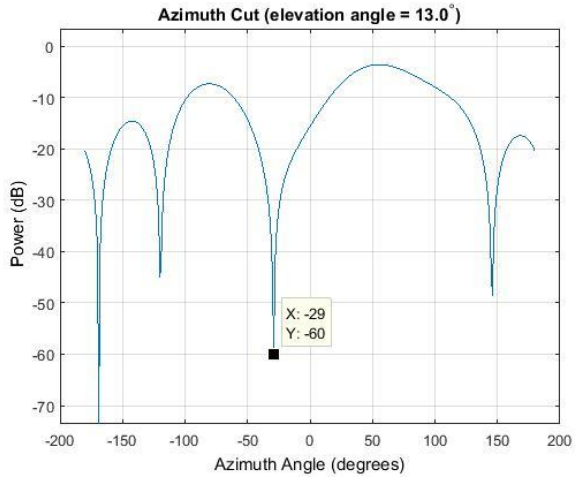

Figure 4-10 Radiation pattern in the plane of jammer source

4.2.2.2 Example Scenario-Two Jammer and One Target Signal

This scenario is exactly same with scenario in section 4.1.2. The target signal is same modulated signal and two jammer sources are again white Gaussian noise. The direction of jammer sources are found with MUSIC algorithm in section 4.2.1.2 and null steering is performed. The radiation pattern in the plane of target signal and received signal after jammer suppression are shown in Figure 4-11. The radiation pattern in the plane of two jammer sources are given in Figure 4-12. From these figures, it can be concluded that null steering shows good suppression performance on jammers and the target modulated signal is extracted.

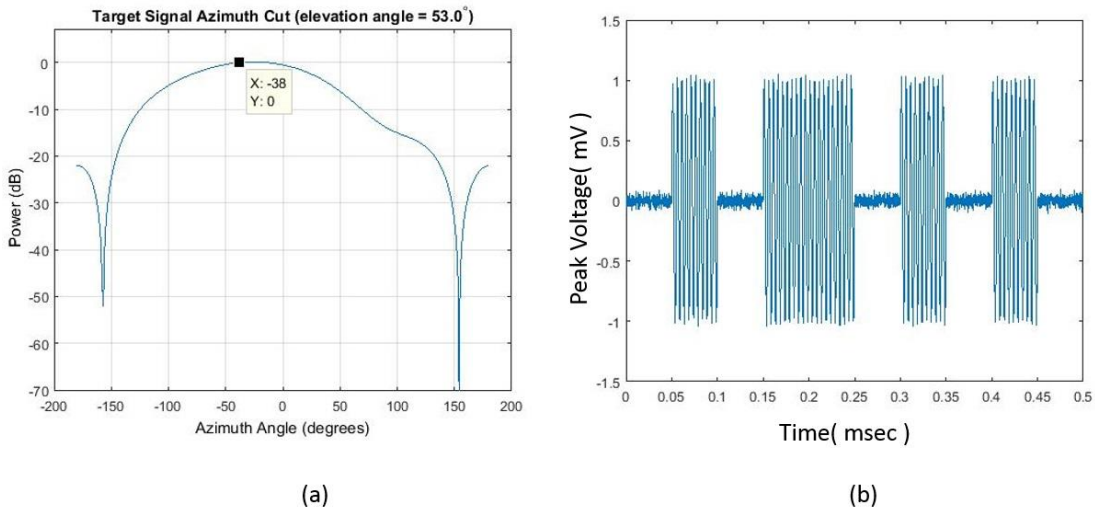

Figure 4-11 a) Radiation pattern toward target signal b) Extracted target signal

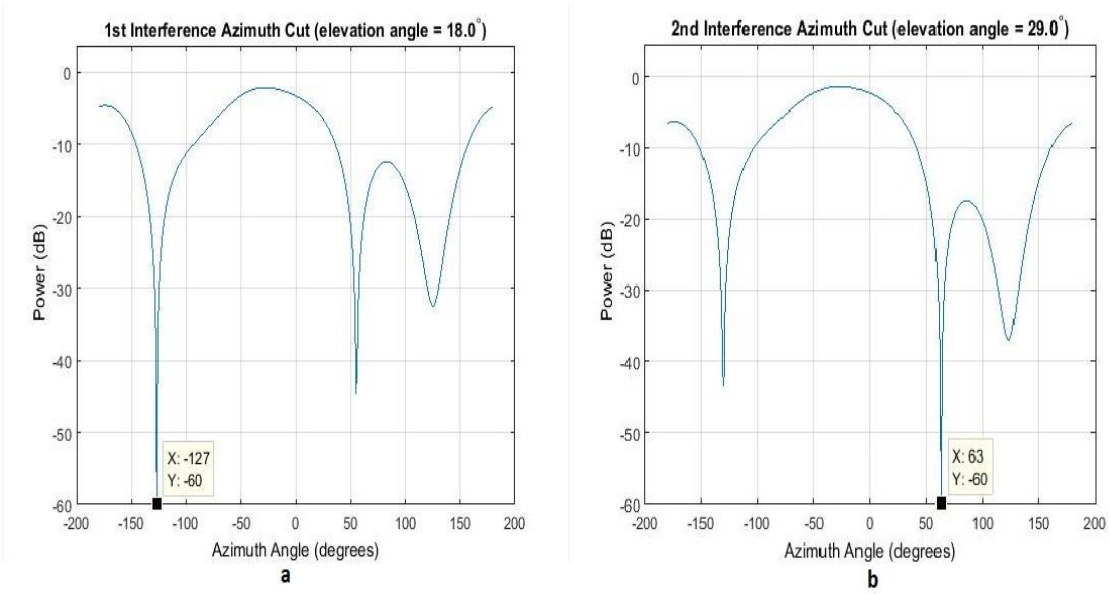

Figure 4-12 a) Radiation Pattern toward 1st Interference b) Radiation Pattern toward 2nd Interference

4.3 Effect of Mutual Coupling on the Performance of Array Signal Processing Algorithms

The mutual coupling also degrades the performance of the array signal processing algorithms [35]. With mutual coupling effect, the radiation pattern of the antenna changes from its isolated value when it is inserted in the array and the pattern of an element in the array environment is called active element pattern. With increasing level

of mutual coupling effect, accuracy of the array factor equation decreases. Therefore, the expected patterns with given weighting coefficients cannot be obtained.

In order to investigate the effect of mutual coupling on the array radiation pattern, a test scenario is formed in MATLAB. In this scenario, two jammer sources are located at azimuth angles [-103^o 86^o] and elevation angles [13^o 34^o]. In addition, the target is placed at -25^o in azimuth and 68^o in elevation. The direction of jammers are found with MUSIC algorithm and the weighting coefficient set to suppress jammer sources is found with application of null steering. I have applied these coefficients to elements of antenna array in CST and observed what type of changes are observed with and without mutual coupling on radiation pattern. The radiation pattern in the plane of target signal is given in Figure 4-13. According to this comparison, it can be said that there is no such a big difference on the radiation pattern toward target signal with or without the mutual coupling effect. The radiation pattern toward 1st and 2nd jammer sources are given in Figure 4-14 and Figure 4-15.According to these comparison results, it can be said that the mutual coupling can seriously decrease the expected suppression performance in desired direction and can shift the position of the null regions that also affect the performance of jammer suppression. In many other scenarios, the weighting coefficient sets are obtained and comparisons are performed in CST. Results were generally same.

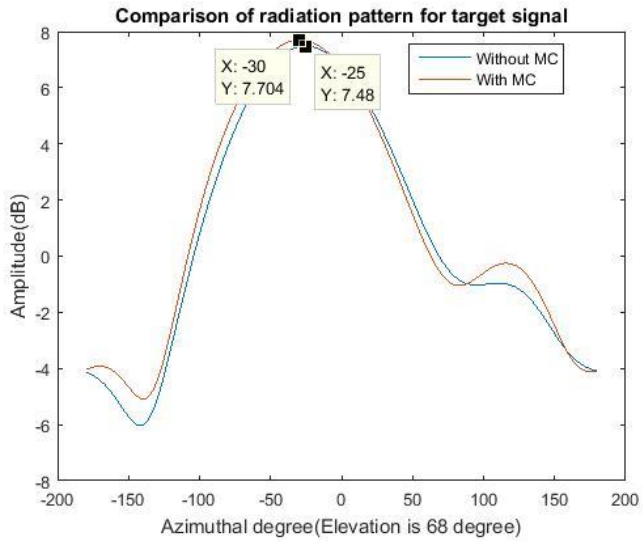

Figure 4-13 Radiation pattern comparison for target signal

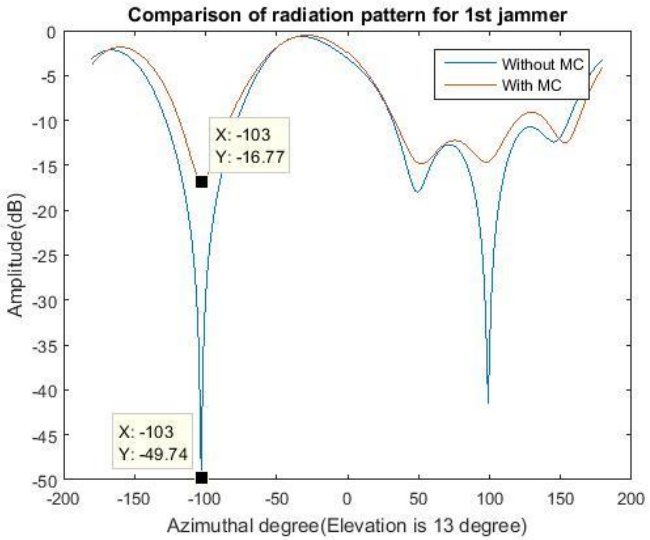

Figure 4-14 Radiation pattern comparison for 1st jammer

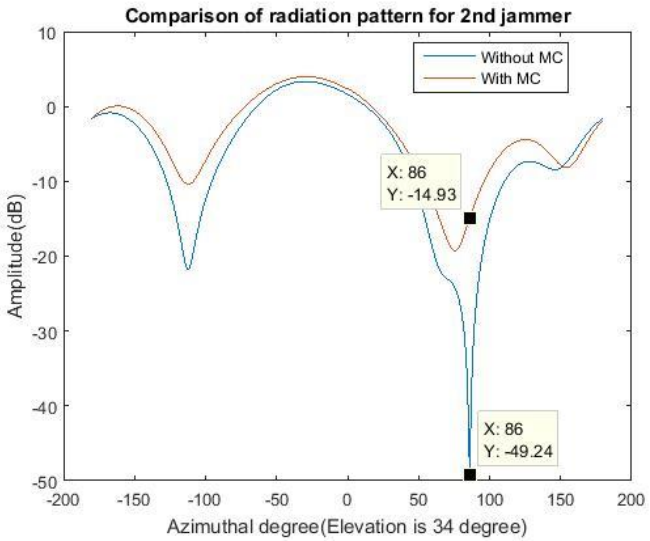

Figure 4-15 Radiation pattern Comparison for 2nd Interference

There are some methods in the literature to compensate the mutual coupling effect to improve array signal processing performance [35],[36],[37]. In this thesis a mutual coupling compensation method is not applied, it is planned as a future work. Moreover, in application of Capon beamforming algorithm, the purpose is to maximize SINR and signals are coming from the antenna elements under mutual coupling effect. Therefore, mutual coupling will not cause any serious decrease in suppression performance of jammer sources for this algorithm. However, in the application of direction finding and then null steering, the algorithms make use of the steering vector which also

neglects mutual coupling effects like AF. Therefore, the accuracy of direction finding algorithm can be affected by mutual coupling and it directly affects the null steering performance.

In this chapter, jammer suppression approaches are studied. Capon beamfoming approach showed similar jammer suppression performance with the null steering approach. Since Capon beamforming approach doesn't need DOA estimation of the jammer sources, it needs lower processing power. This is one of the advantage of Capon beamforming approach. If DOA estimation and null steering are used together, there will be possibility to estimate positions of the jammers by using multiple sensor systems. In usage of null steering algorithm, the DOA estimation performance is very important. If there is mismatch between real coming direction and estimated one, null regions will be directed towards wrong places and jammers can't be suppressed. When there is mismatch between the real incoming direction and estimated direction of the target signal, it is possible to increase the performance of the Capon beamforming approach by using robust Capon techniques [38].

In theory, with *n* element antenna array design, it is possible to suppress *n-1* jammer sources at the same time by giving only one target signal direction. However, in MATLAB simulations, it is observed that the performance of beamforming algorithms degrades considerably as the number of jammers increases. It is also observed that it is not possible to suppress 3 jammers successfully with a 4 element antenna array. Another factor that affects the suppression performance is the angular separation between the jammer and target signals. When the angle between jammer and target source is below 15^{o}, beamforming algorithms give inapplicable coefficient set and jammers cannot be suppressed.

CHAPTER 5

EXPERIMENTS WITH REAL SETUP

In this thesis, active GPS antenna array design and measurements are discussed with subsections. In addition, beamforming is placed in one chapter in order to get insight about the theory and MATLAB simulations of implemented algorithms. In this chapter, there will be GPS antijamming experiments with real time test setup. Two types of experiments are applied step by step. These experiments can be named as postprocessing of real data in MATLAB and experiments in real environments with live GPS and jammers. It should be noted that, the contribution of my colleague Fatih Erdem in the development of test environment was so important.

5.1 Post Processing of Real Data in Matlab

With this test procedure, it is aimed to see performances of the previously discussed beamforming algorithms on the real signal sources. For that purpose, I have used active antenna array, transmitters, receiver and recording device. The diagram that provide some insight about this experiment is shown in Figure 5-1.

In order to test the performance of Capon beamforming algorithm, different scenarios are created with one target and one constant jammer, one target and two constant jammer and one target and one mobile jammer. The serial data (10101010101…10) is used to modulate carrier with on-off keying by repeating in each seconds. Then this modulated signal as the target signal in order to see whether bit error exist or not after jammer suppression. Continuous wave jammer is used as a jammer source. In one of the test scenarios, target signal broadcasting as started at the beginning. Then record is started. After 1.5 s later than the beginning of record, the jammer is activated for 2 seconds and then it is closed again.

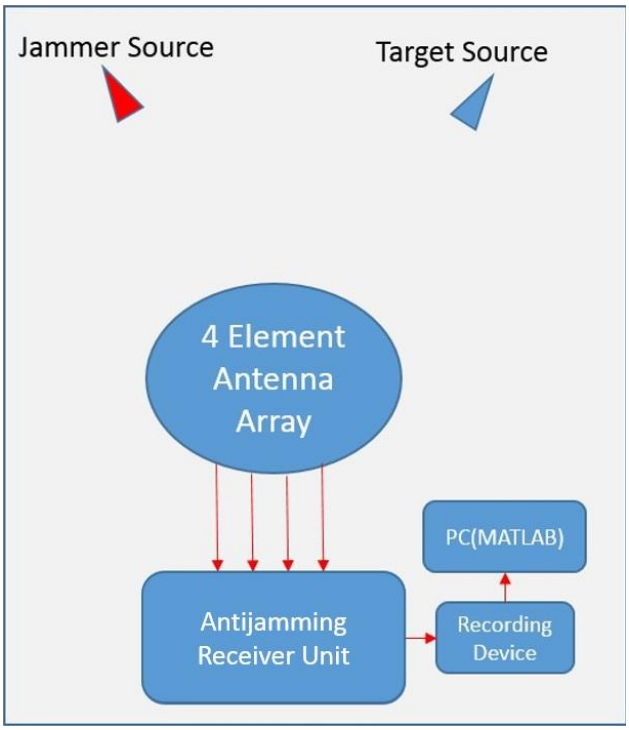

Figure 5-1 Antijamming tests on recorded data

The serial valuable information is repeated in every second during this record. The recorded data in one of the antennas in array is shown in Figure 5-2. In this figure, the repeated valid signal in every one second is shown around 4.45 seconds as an example. Normally, this valuable signal should be obvious around 2.45 seconds. However, the jammer is active in this region and there is no data. In other words, the jammer successfully jammed the target signal. The Capon beamforming approach was applied on the received data taken from 4 element array and the output of the beamformer is taken as shown in Figure 5-3. It can be seen from the output signal that, the data which was disappeared under jamming is extracted. When the output data is investigated in detail, it is concluded that the data is obtained without any bit error. In application of Capon beamforming algorithm, I noticed that the taken number of snapshot while calculating autocorrelation function is very important. In MATLAB simulations, increasing number of snapshot increases the jammer suppression performance. However, process of jammed signal with sub-blocks provide higher suppression rates.

Capon beamforming algorithms is applied on many test scenarios that include constant jammer, mobile jammer and multiple jammer. In these tests, Capon algorithm has successively extracted the valid data with varying suppression ratios. The jamming

suppression performance on these tests was between 25 and 40 dB. When the suppression level is around 25 dB, the valid data may not be visually observed but the accuracy of the extracted data can be measured from the autocorrelation of the jammer suppressed data and the reference data signal.

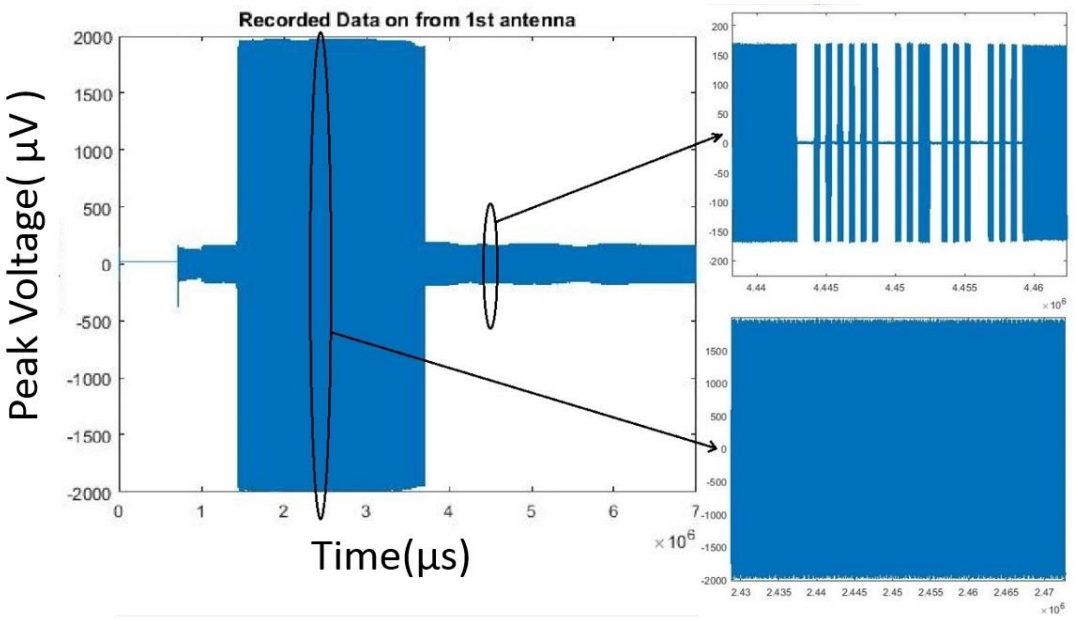

Figure 5-2 Recorded data on antenna 1 under constant jamming threat

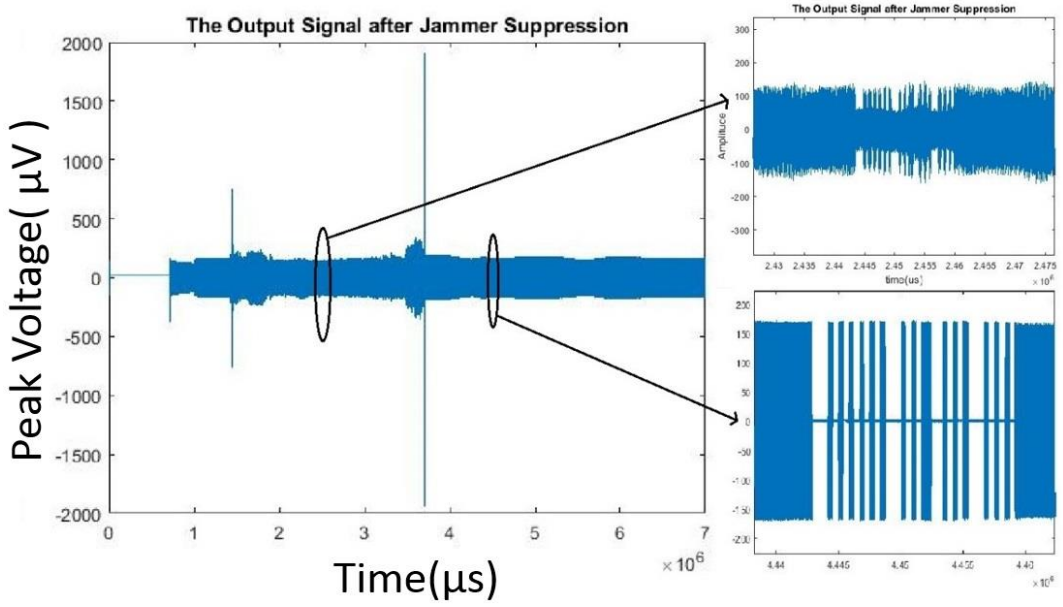

Figure 5-3 Output of the Capon beamformer

Another beamforming approach that is used in this thesis is the combination of the DOA estimation with MUSIC algorithm and null steering algorithm. In order to test these algorithms, only jammer signal is used and it is aimed to estimate DOA of this source and suppress it. In one of the test scenarios, the jammer signal is applied from 180^o azimuth and 60^o elevation angle. MUSIC algorithm is applied to specific time interval of the received data. In Figure 5-4, the recorded data with 1st antenna is given. The MUSIC algorithm is applied between 2.865s and 2.869 s. The MUSIC spectrum is found as shown in Figure 5-5. Peak is not as sharp as the one observed in MATLAB simulations. This might be due to several effects such as multipath and mutual coupling. The peak of the MUSIC spectrum is at 170^o azimuth and 59^o elevation angles. From this incoming angle information of jammer, null steering algorithm is applied through previously determined specific portion of the recorded data and the output is shown in the right bottom side of Figure 5-4.

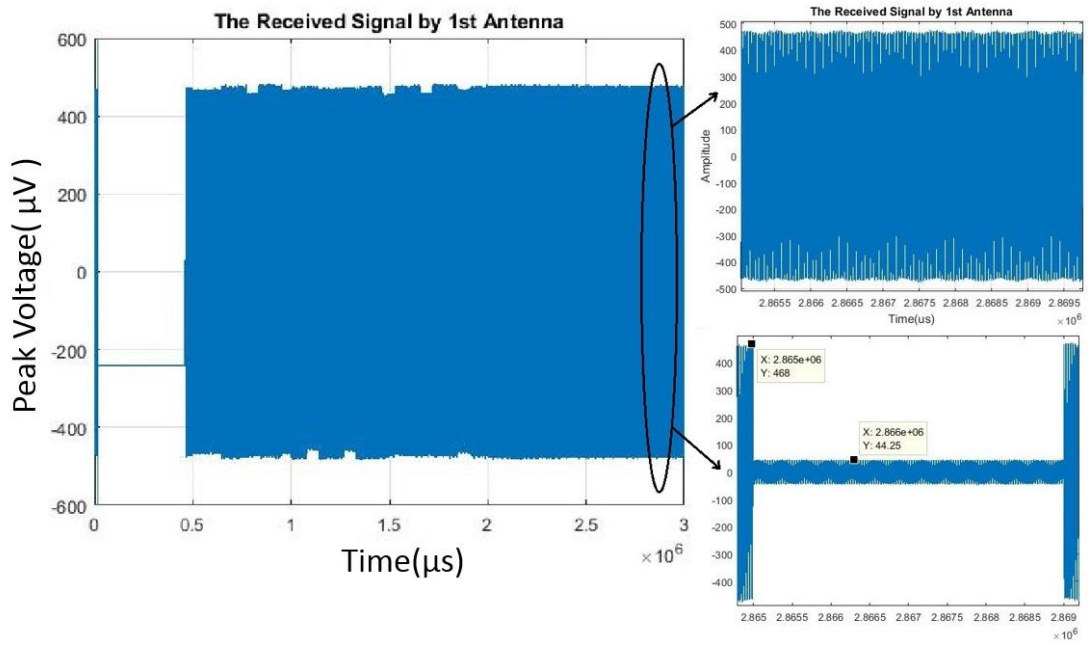

Figure 5-4 Recorded data on antenna 1 under constant jamming threat

In experiments for DOA estimation and null steering, it is noticed that the DOA estimation accuracy can seriously degrade in some cases. In this situations, jammer suppression with null steering performance is also degraded. It can be noted that the relation between number of jammer sources and the amplitudes of eigenvalues is

verified in experiments. When the DOA accuracy is high, the null steering performance varied between 20 and 30 dB. Because the tests of DOA estimation and null steering on recorded data didn't give perfect results, it is decided to use only Capon beamforming algorithm in real time GPS antijamming tests.

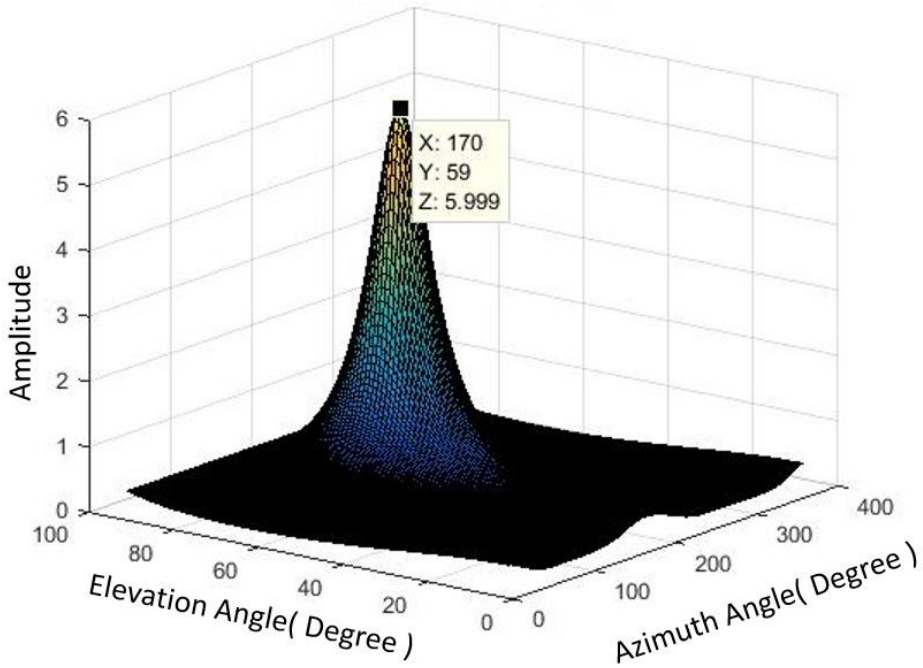

Figure 5-5 MUSIC spectrum under 1 jammer source

5.2 Experiments in Real Environments with Live GPS and Jammer Sources

With this thesis work, the main purpose is to develop such a system that can detect the existence of GPS jammer source, suppress it and transmit the clean GPS signal to any commercial GPS receiver. In this part, real time GPS anti-jamming performance of the system that is discussed in this thesis will be investigated. In this experiment, the antenna was located in outside and real jammer source was used. All tests are performed in real time by calculating and applying complex coefficients to digitized data in ARM processor. A commercial GPS receiver that includes SirfStar chipset is used. In order to see the situations of satellites under jamming and after jamming suppression, the Visual GPS View program is used. In addition to that, the suppression rates are observed by connecting output of the antijamming receiver platform to

spectrum analyzer. The overall block diagram about the real time antijamming tests is shown in Figure 5-6.

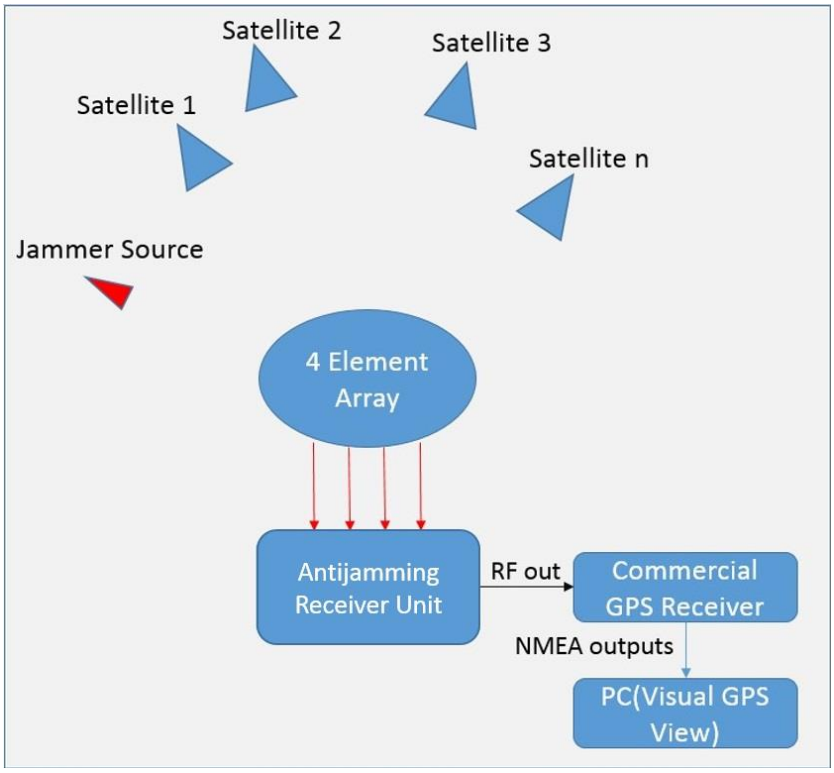

Figure 5-6 Real time GPS antijamming tests

In introduction part of this thesis, the self-resistance of the GPS receivers due to code gain is discussed. This code gain may show small differences from receiver to receiver. In order to measure the code gain of receiver that is used in real time antijamming test, some measurements in controlled environment are performed according to block diagram that is shown in Figure 5-7. According to this measurement the GPS antenna is placed to outside. The GPS antenna output is combined with tunable CW jammer source. Then, the output of the combiner is divided two output. One of the output is connected to spectrum analyzer in order to see power level of the jammer and other output is connected to GPS receiver. GPS receiver is connected to PC and the health of the satellites under jamming source with increasing power level is observed. According to measurements, the receiver lose the tracked satellite after 50dB J/S ratio if we take the GPS signal level as -130 dBm. The J/S level of different jammers w.r.t. change in distance is investigated in [3] and the 50dB J/S resistance is placed on these

values as shown in Figure 5-8. According to this figure, jammer with 10mW output power can jam my receiver from 550 m.

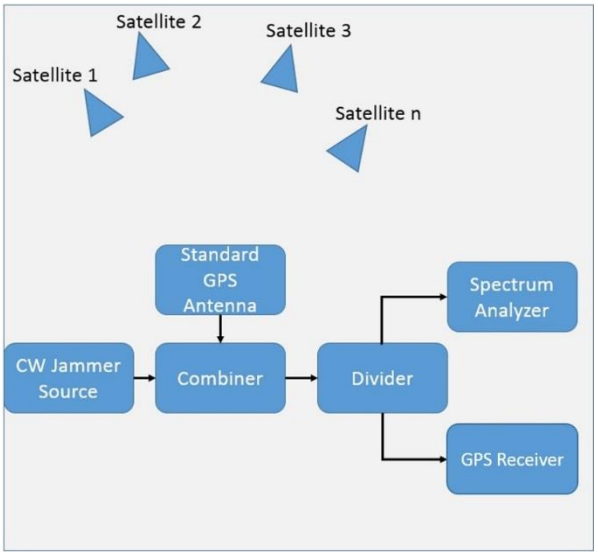

Figure 5-7 GPS receiver self-resistance measurement

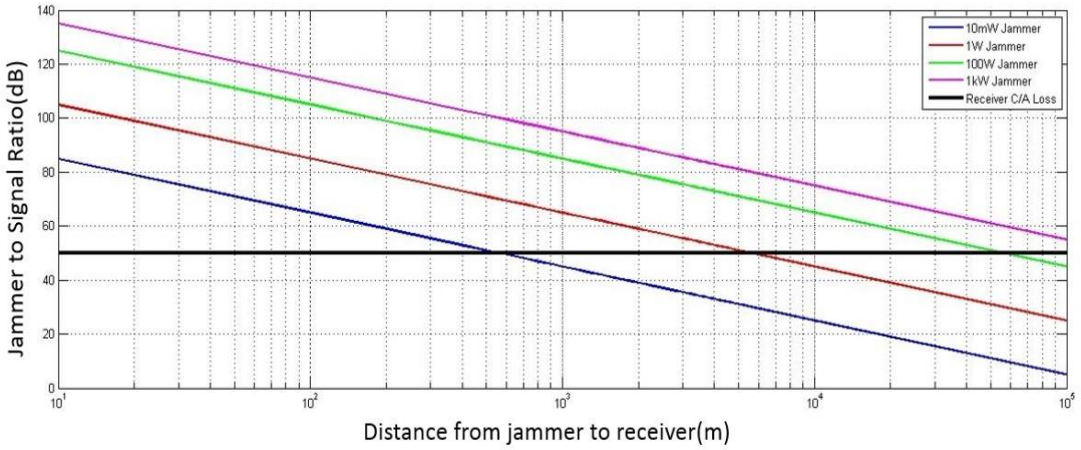

Figure 5-8 J/S Ratio of different jammers w.r.t.change in distance

As discussed in previous part, Capon beamforming algorithm is the only anti-jamming algorithm used in real time antijamming tests. During many test scenarios with varying jammer locations, the real time antijamming system that is shown in Figure 5-6 is performed and GPS jammer suppression has successfully performed. In these tests,

jammer suppression level changed between 30-35 dB and GPS operation was continued under jamming threat.

In this section, results of one of the scenarios is shared. In this scenario, the active antenna array is located outside and jammer is placed such that it looks toward the antenna array. At the beginning of test, the jammer was inactive and GPS satellites were acquired and tracking was started with 9 satellites. After 10 seconds later jammer become activated and all the tracked satellites have become lost. When jammer was activated, the real time system was detected it and started the antijamming operation. After application of beamforming, the jammer was suppressed and all of the previously tracked satellites become visible again with smaller power level. The code gain for the tracked satellites during this test is shown in Figure 5-9. As you can see, at the beginning of test, there are nine tracked satellites and the situations of these satellites when the jammer is inactive is also shown in Figure 5-10. When jammer is activated, there is no tracked satellites and the situation of satellites is also shown in Figure 5-11. The waiting time about 10 seconds can be decreased with defining it in software. This waiting time is kept a bit longer due to better observation in jammer active region. In this test, the jammer power level is suppressed 35 dB and after jammer suppression all of the previously tracked nine satellites have become visible again. The power level of the tracked satellites after jammer suppression is also shown in Figure 5-12.

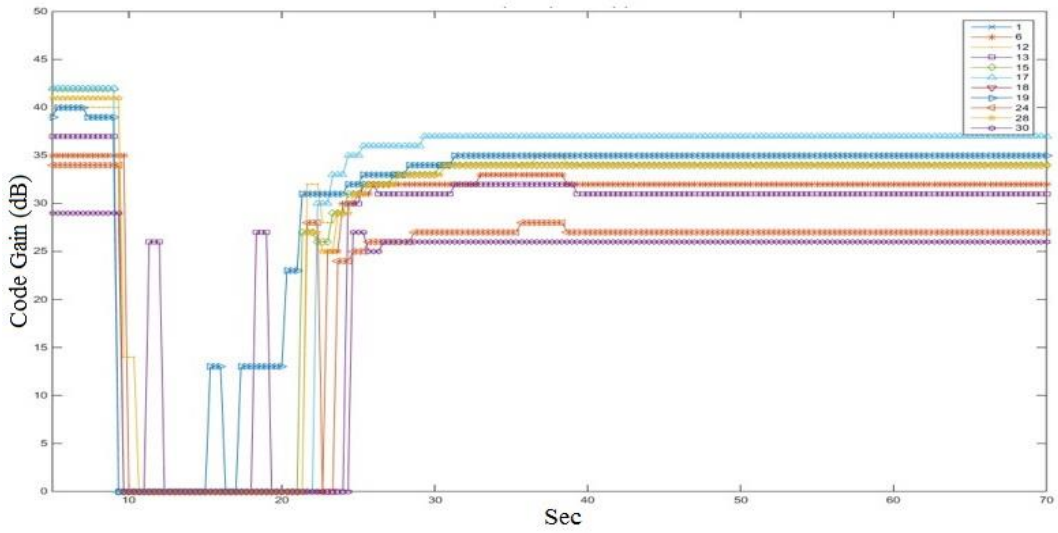

Figure 5-9 Code gain levels for the tracked satellites

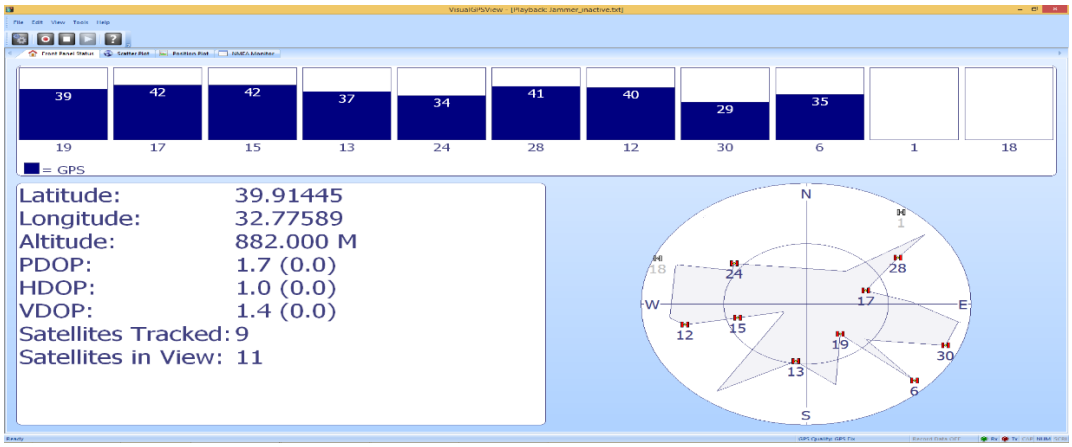

Figure 5-10 Power levels of tracked satellites in jammer inactive region

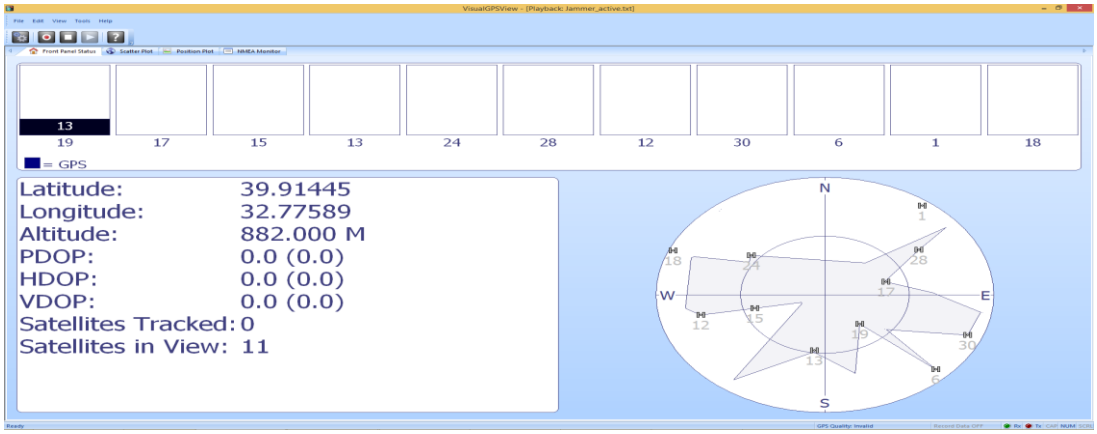

Figure 5-11 Power levels of tracked satellites in jammer active region

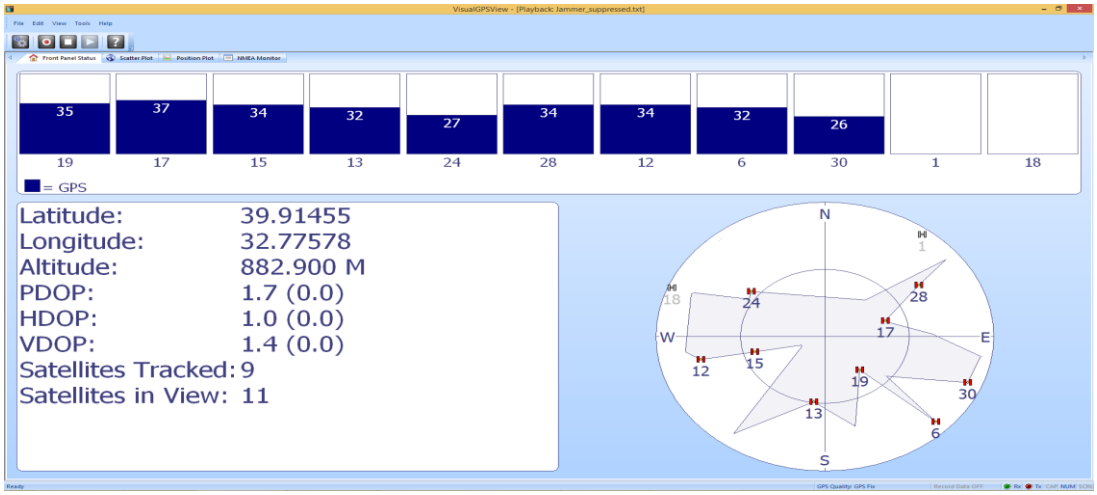

Figure 5-12 Power Levels of Tracked Satellites after Jammer Suppression

In real time GPS antijamming tests, it is observed that the jamming suppression level varied between 30-35 dB. When this suppression level is put above the self-resistance

of GPS receiver, the resistance of the receiver increases from 50 dB J/S ratio to 85 dB J/S ratio. In Figure 5-13, the external 35dB protection of the proposed GPS antijamming system is added to 50 dB self-resistance of the GPS receiver. According to this figure, a jammer with 1W output power level can jam the standalone GPS receiver from 5 km. With 35dB external resistance, the same jammer can jam the receiver from only 100 m. This improvement shows the importance of antijamming systems for GPS receivers. The jamming concept cannot be completely disappeared but antijamming systems may get some extra protection and provide GPS service up to some higher jammer power levels.

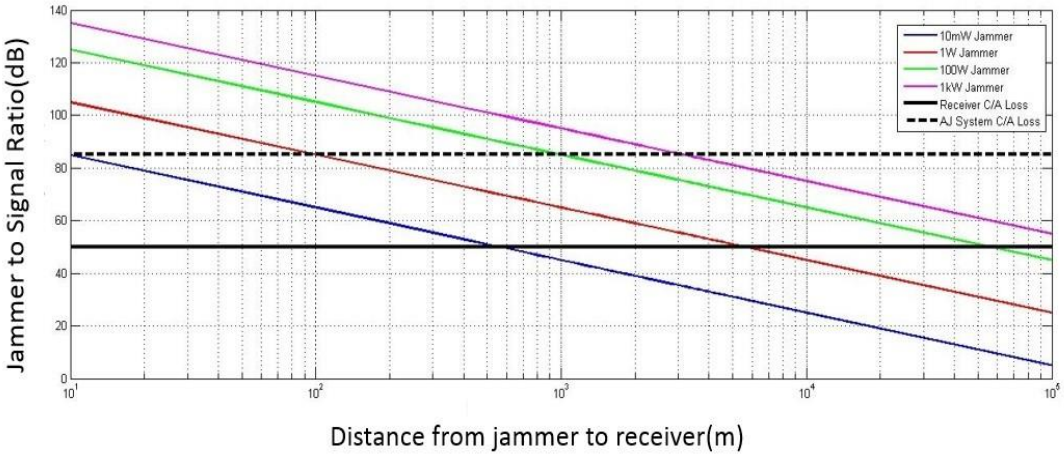

Figure 5-13 J/S ratio of different jammers wrt. change in distance

CHAPTER 6

CONCLUSION

In this thesis, GPS jamming suppression system with four element active antenna array design and implementation of beamforming algorithms are discussed. The main motivation of this thesis is to create awareness about the importance of GPS jamming threat and design an alternative system with much lower cost according to equivalent products summarized in the introduction. The work on the antenna array design and implementation of beamforming algorithms have progressed in parallel. The most important section of this thesis is the active antenna array design that is performed step by step. First of all, nearly square microstrip design is chosen as a GPS antenna in order to achieve circular polarization. For antenna design, RO4003 material was chosen. Simulations of the designed antennas were performed in CST MS. Manufacturing and measurements was performed in Ayaslı Research Center. After manufacturing and measurements of one antenna element, 4 element array design and manufacturing were performed. After measurements, it was noticed that measurements of the array elements were slightly shifted from the measurements of the reference element. The potential reason for this shift was the mutual coupling effect between array elements. Although 10 dB impedance bandwidth of the elements in the array included the GPS L1 band, antennas were not circularly polarized in this band. Then increase in bandwidth of the antenna was tried in order to compensate the potential shift in the target center frequency due to mutual coupling. For that purpose, new antenna was designed and manufactured with thicker substrate. This new antenna has nearly two times bandwidth of the antenna with thinner bandwidth. However, the center frequency of the antenna was again shifted from the target center frequency and tuning was necessary for that antenna. The supplementary part of the active antenna array design was the amplifier unit. LNAs were placed just after the antenna in order to decrease the overall noise figure as in most communication systems. Therefore, it

is decided to make a compact design for a card with four channels on it and integrate with the antenna array. After the design, manufacturing and tests stages of the LNA card, the four element active antenna design was completed.

Spatial suppression of the GPS jammers is possible by adaptively changing the radiation pattern of the antenna array. This is possible by multiplying each channel with complex coefficients. These complex coefficients are named as weighting coefficients. In order to find these coefficients, beamforming algorithms were used. In this thesis, two main approaches that are Capon beamforming and null steering are used. The purpose of Capon beamforming algorithms is to maximize SINR. Only necessity while performing this algorithm is the direction of the target signal. In GPS antijamming system, the targets are GPS satellites and their position information is known from the almanac data. This algorithm can adaptively suppress the jammer source. In application of null steering, both target signal direction and jammer direction is needed. In order to obtain the jammer signal direction, I have used MUSIC direction finding algorithm. Jammer suppression performances of these two systems (which are mostly close) can be found in Chapter 4. However, after doing experiments using with experiments using real signal sources and processing of offline data in MATLAB, it is decided that use of Capon algorithms is better option due to its higher suppression rate and more stable performance. Therefore, only this algorithm was used in real time GPS antijamming tests. In real time antijamming tests, active antenna array and antijamming receiver system runs the beamforming algorithms were used. In these real time tests, CW jammer was applied from different directions according to the antenna array. When jammer was activated, the GPS receiver lost the satellites and GPS positioning stopped. The antijamming system has detected the existence of a jammer source and applied suppression in the jammer direction. Suppression levels were varied between 30-35 dB. After jammer suppression, GPS satellites have become visible again and positioning operation continued.

In this part, all works that were performed during this thesis are summarized. At the beginning of this work, the purpose was to construct an active GPS antenna array and achieve real time GPS antijamming by using this array and beamforming algorithms. At this point, it can be said that this purpose is achieved. Of course there are a lot of things to do for future work. Compensation of mutual coupling in order to increase jammer suppression performance, designing antennas with wider bandwidth

in order to cover multiple satellite system, designing dual band antennas to cover both L1 and L2 band of the GPS, increasing number of the antenna elements in the system to get higher angle resolution, improvement in suppression performance and implementation of new beamforming methods to suppress different types of jammers can be counted as a potential future work of this thesis.

REFERENCES

[1] Mendizaba, S.J., Berenguer, R., & Melendez,J.(2009). *GPS and GALILEO: Dual RF Front-End Receiver Design, Fabrication and Test*. New York: McGraw-Hill

[2] Borre,K. (2006). *A Software-Defined GPS and GALILEO Receiver: A single-frequency approach*. Boston: Birkhauser

[3] M.Jones, "Protecting GNSS Receivers from Interference and Jamming," *Inside GNSS*, pp.40-49, March/April 2011

[4] Kraus,T., Bauernfeind, R., Eissfeller, B.,"Survey of In-Car Jammers –Analysis and Modeling of the RF signals and IF samples," *ION GNSS 2011*, Portland, OR, USA, 19-23 Sept., 2011.

[5] P.F.MacDoran, "GNSS Interference and Attack Mitigation," Loctronix, GPS World, 2008

[6] Paonni. M, "Wavelets and Notch Filtering, Innovative Techniques for Mitigation RF Interference", *Inside GNSS*, pp.54-62, January/February 2011

[7] *Multi-constellation and Multi-Frequency*, Retrieved from: www.novatel.com/an-introduction-to-gnss/chapter-5-resolving-errors/multi-constellation-and-multi-frequency/(October,2014)

[8] C.Fernandez-Prades, J.Arribas and P.Closas, "Robust GNSS Receivers by Array Signal Processing: Theory and Implementation," *in Proceedings of the IEEE*, vol.104, no.6, pp.1207-1220, June 2016

[9] *Single-Enclosure GPS Anti-Jam Technology(GAJT)*. Retrieved from http://www.novatel.com/assets/Documents/Papers/GAJT-700ML.pdf

[10] *Digital Integrated GPS Anti-Jam Receiver(DIGAR).* Retrieved from http://www.rockwellcollins.com

[11] *TopShield, The Ultimate GPS Anti-Jam Solution*. Retrieved from http://www.thalesgroup.com

[12] *Anti-Jam GPS Antennas.* Retrieved from http://www.baesystems.com

[13] CST Microvawe Studio[Computer Software].(2014). Retrieved from http://www.cst.com,(October,2014)

[14] Zeng.Y, (2008), *Adaptive Antenna Array Processing for GPS Receiver*, Master Thesis, The University of Adelaide Australia

[15] Tuncer,E.T. , Friedlander,B.(Eds.) (2009). *Classical and Modern Direction-of-Arrival Estimation.* Burlington,USA: Elsevier

[16] MATLAB[Computer Software].(2015).Retrieved from http://www.mathworks .com,(October,2014)

[17] Neff,H.P.(1991). *Introductory electromagnetics*. New York: Wiley.

[18] Chen,X. (2012). *Antennas for global navigation satellite systems*. Chichester, West Sussex, U.K: John Wiley et Sons.

[19] Balanis,C.A.(2005). *Antenna Theory: Analysis and Design.* Hoboken, NJ:Wiley Interscience.

[20] Garg,R.(2001). *Microstrip Antenna Design Handbook*. Boston,MA:Arteck House.

[21] E.O.Hammerstad, "Equations for Microstrip Circuit Design," *Proc.Fifth European Microvawe Conf.*, pp.268-272, September 1975

[22] Bahl, I.J., & Bhartia,P.(1980). *Microstrip Antennas*, Dedham, Mass: Artech House.

[23] Circular polarization. Retrieved from: http://hyperphysics.phy-astr.gsu.edu/hbase/phyopt/polclas.html

[24] K.R.Carver and J.W.Mink, "Microstrip Antenna Technology," *IEEE Trans.Antennas Propagat.*, Vol.AP-29, No.1, pp.2-24,January 1981.

[25] Lee,S.K., Sambell,A., Korolkiewicz,E., Loh,S.F.,Ooi,S.F.,&Qin,Y. "A design procedure for a circular polarized, nearly square patch antenna," *Microwave Journal*,48,1,116-129, January 2005.

[26] Y.T.Lo, B.Engst, R.Q.Lee, "Simple Design Formulas for Circularly Polarized Microstrip Antennas," *IEE Proceedings*, Vol.135,Pt.H,No.3,June 1998

[27] William L.Langston "Impedance, Axial-Ratio and Receive-Power Bandwidths of Microstrip Antennas," *IEEE Transactions on Antennas and Propagation*, Vol.52, No.10, October 2004

[28] *Antenna array basics*. Retrieved from www.antenna-theory.com/arrays/main.php#arrays(April,2015)

[29] *Monolithic Amplifier*. Retrieved from www.minicircuits.com/PMA4-33GLN+, (May,2015)

[30] J.Capon, "High Resolution Frequency Wavenumber Spectrum Analysis," *Proc.IEEE*,Vol.57,pp1408-1418, Aug.1969

[31] P.W.Howells, "Intermediate Frequency Sidelobe Canceler," Technical Report, U.S Patent 3202990 , May 1959.

[32] S.P.Applebaum, "Adaptive Arrays," *IEEE Trans. Antennas and Propagation*, 24:585-595, September 1976.

[33] H.Trees, *Optimum Array Processing, Detection, Estimation and Modulation Part 4*, John Wiley&Sons, New York,2002

[34] Joshi R, Dhande A, "Direction of Arrival Estimation with Using Music Algorithm",*IJRET*, Volume:03, Issue:03, Mar-2014

[35] H.S.Lui, H.T.Hui,M.S.Leong, "A note on the mutual coupling problems in transmitting and receiving antenna arrays," *IEEE antennas and propagation magazine*, Vol.51, No.5, October 2009

[36] H.T.Hui, "Improved Compensation for the Mutual Coupling Effect in a Dipole Array for Direction Finding," *IEEE Transactions on Antenna and Propagation*, AP-51,9, September 2003 pp.2498-2503.

[37] H.Steyskal, J.S.Herd, "Mutual Coupling Compensation in Small Array Antennas," *IEEE Transactions on Antennas and Propagation*, Vol.38, No.12, December 1990

[38] P. Stoica, Zhisong Wang and Jian Li, "Robust Capon beamforming," in *IEEE Signal Processing Letters*, vol. 10, no. 6, pp. 172-175, June 2003